

SHIP DETECTION USING SYNTHETIC APERTURE RADAR IMAGERY

*A Project report submitted in partial fulfillment of the requirements for
the award of the degree of*

**BACHELOR OF TECHNOLOGY
IN
ELECTRONICS AND COMMUNICATION ENGINEERING**

Submitted by

B.Nikhil (317126512124)

M. Kalyan Ram(317126512149)

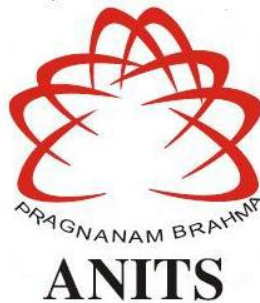
J. Meher Pranav (317126512137)

V. S .S. Puneeth(317126512176)

Under the guidance of

Mrs.V.Shireesha M.Tech(Ph.D)

Assistant Professor



DEPARTMENT OF ELECTRONICS AND COMMUNICATION ENGINEERING

**ANIL NEERUKONDA INSTITUTE OF TECHNOLOGY AND SCIENCES
(UGC AUTONOMOUS)**

*(Permanently Affiliated to AU, Approved by AICTE and Accredited by NBA & NAAC with 'A' Grade)
Sangivalasa, bheemili mandal, visakhapatnam dist.(A.P)*

2020-2021

DEPARTMENT OF ELECTRONICS AND COMMUNICATION ENGINEERING

**DEPARTMENT OF ELECTRONICS AND COMMUNICATION ENGINEERING
ANIL NEERUKONDA INSTITUTE OF TECHNOLOGY AND SCIENCES
(UGC AUTONOMOUS)**

*(Permanently Affiliated to AU, Approved by AICTE and Accredited by NBA & NAAC with
'A' Grade)*

Sangivalasa, Bheemili mandal, Visakhapatnam dist (A.P)



CERTIFICATE

This is to certify that the project report entitled "SHIP DETECTION USING SYNTHETIC APERTURE RADAR IMAGERY" submitted by B.NIKHIL(317126512124), J.MEHER PRANAV(317126512137), M.KALYAN RAM (317126512149), V.S.S.PUNEETH(317126512176) in partial fulfillment of the requirements for the award of the degree of Bachelor of Technology in Electronics & Communication Engineering of Andhra University, Visakhapatnam is a record of bonafide work carried out under my guidance and supervision.



Project Guide

Mrs.V.Shireesha

Assistant Professor

Department of E.C.E

ANITS

Assistant Professor
Department of E.C.E.
Anil Neerukonda
Institute of Technology & Sciences



Head of the Department

Dr. V. Rajyalakshmi

Professor & HOD

Department of E.C.E

ANITS
Head of the Department
Department of E C E

Anil Neerukonda Institute of Technology & Sciences
Sangivalasa - 531 162

ACKNOWLEDGEMENT

We would like to express our deep gratitude to our project guide **Mrs.V.Shireesha** Assistant Professor, Department of Electronics and Communication Engineering, ANITS, for her guidance with unsurpassed knowledge and immense encouragement. We are grateful to **Dr V. Rajyalakshmi**, Head of the Department, Electronics and Communication Engineering, for providing us with the required facilities for the completion of the project work.

We are very much thankful to the **Principal and Management, ANITS, Sangivalasa**, for their encouragement and cooperation to carry out this work.

We express our thanks to all **teaching faculty** of Department of ECE, whose suggestions during reviews helped us in accomplishment of our project. We would like to thank **all non-teaching staff** of the Department of ECE, ANITS for providing great assistance in accomplishment of our project.

We would like to thank our parents, friends, and classmates for their encouragement throughout our project period. At last but not the least, we thank everyone for supporting us directly or indirectly in completing this project successfully.

PROJECT STUDENTS

**B.Nikhil (317126512124),
J.Meher Pranav (317126512137),
M.Kalyan Ram (317126512149),
V.S.S.Puneeth (317126512176)**

ABSTRACT

Synthetic Aperture Radar (SAR) is a high-resolution ground-mapping technique with the ability to effectively synthesize a large radar antenna by processing the phase of a smaller radar antenna on a moving platform like an airplane or a satellite. SAR images, due to its properties, have been the focus of many applications such as land and sea monitoring, remote sensing, mapping of surfaces, weather forecasting, among many others. Their relevance is increasing on a daily basis, thus it's crucial to apply the best suitable method or technique to each type of data collected.

Several techniques have been published in the literature so far to enhance automatic ship detection using Synthetic Aperture Radar (SAR) images, like multilook imaging techniques, polarization techniques, Constant False Alarm Rate (CFAR) techniques, Amplitude Change Detection (ACD) techniques among many others. Depending on how the information is gathered and processed, each technique presents different performance and results. Nowadays there are several ongoing SAR missions, and the need to improve ship detection, oil-spills or any kind of sea activity is fundamental to preserve and promote navigation safety as well as constant and accurate monitoring of the surroundings, for example, detection of illegal fishing activities, pollution or drug trafficking.

The main objective of this Report is to study and implement a set of algorithms for automatic ship detection using SAR images from Sentinel-1 due to its characteristics as well as its ease access.

CONTENTS

CHAPTER 1	Introduction	Pg.No
1.1	SAR Technology Use and Applications	1
1.2	Problem Statement	2
1.3	Aim and Scope	3
1.4	Report Structure	4
CHAPTER 2	State of Art	
2.1	Historical Framework and Applicability	5
2.2	Basic Concepts And SAR Properties	11
2.3	SAR Systems Radar Equation	12
2.4	SAR Geometry and Acquisition	14
2.5	SAR Processing and Factors that affect Its Image	19
2.6	Ships Detection	19
2.7	Multi-look Imaging techniques	21
2.8	Constant False Alarm Rate techniques	25
2.9	Polarization techniques	29
2.10	Amplitude Change Detection techniques	32
CHAPTER 3	Techniques Evaluation And Selection	
3.1	Basic Guidelines	36
3.2	Technique selection	39
3.3	Data Analysis	39
3.4	Scenario of application	44

CHAPTER 4	THE ALGORITHMS	
4.1	Introduction	46
4.2	Read Data processing function	48
4.3	The dynamic Division processing function	49
4.4	Gaussian CFAR function	51
4.5	K-means with Gaussian CFAR function	56
4.6	Contact Type and Results	59
CHAPTER 5	Simulation Results	60
CHAPTER 6	Conclusion	62
References		63
Appendix		65

LIST OF FIGURES

FIGURES		PG.NO
1	Major SAR Satellites timeline	6
2	Tx/Rx of a satellite	12
3	Illustration of the Tx/Rx process of a radar signal	13
4	SAR Strip Map geometry	14
5	Simulation of a Synthetic Aperture	14
6	StripMap mode (SM)	15
7	InSAR mode	17
8	Spotlight mode	18
9	ISAR mode	20
10	SCANSAR mode	21
11	SAR Geometry	22
12	Synthetic aperture split process	22
13	Detection of a moving target	23
14	RADARSAT-1 data set visualization and specs	24
15	Results obtained and explanation of the use different windows	25
16	Target Area for analysis	26
17	Ship Detection based on CFAR algorithms. (a) - alpha stable distribution; (b) - Weibull distribution and (c) - K-distribution	27
18	Block Diagram of Segmentation based CFAR algorithm	27
19	San Francisco Bay, USA. (a) Google Earth image of the area (b) Pauli RGB image of the RADARSAT-2 fully	29

	polarimetric data set	
20	(a) Nautical chart showing buoys positions. (b) - (f) Maps of the DoP over San Francisco Bay in different hybrid/compact and linear dual-pol modes. (b) HH-HV. (c) VH - VV. (d) HH-VV. (e) CL-pol. (f) /4.	30
21	(a) Pauli RGB image of test area from San Francisco Bay, RADARSAT-2 fully polarimetric data set. (b) - (f) Maps of DoP over the test area in diferent hybrid/compact and linear dual-pol modes. (b) HH-VV. (c) VH-VV. (d) HH-VV. (e) CL-pol. (e) /4. (g) ship Detection results, based on quad-pol data	31
22	Pauli RGB image of the NASA/JPL UAVSAR fully polarimetric dataset from the Deep water Horizon oil spill in northern Gulf of Mexico,USA	32
23	Oil-slick property/type recognition using the Dop (DB) in dual-pol SAR. (a) VH-VV. (b) HH-VV. (c) CL-pol. (d) . The region is a subset of UAVSAR data set	32
24	SAR Amplitude Change Detection processing chain starting fromdetected input products	33
25	Pairwise ACD applied to RADARSAT-2 XF data for harbour monitoring near Murmansk. Chip size is +/- 2.3 x 1.3 km	34
26	Time Series applied to RADARSAT-2 XF data for infrastructuremonitoring. Top Image: Radar change map; Middle Image: orthophoto from Bundesant für Kartographie und Geodäsie; Bottom Image: SAR time series at location A	35
27	Illustration of a phased array	40
28	Sentinel 1 operating modes	41

29	Processing Flow	42
30	Graphical Representation of Sentinel-1 Core Products	43
31	IW products. Left side is IW SLC bursts and sub swaths. Right side is the IW GRD product	44
32	Portugal EEZ and the proposed platform extension	45
33	Comercial Routes around the World	45
34	Algorithm's Interaction structure	46
35	SNAP Operations and Configurations	47
36	Sentinel SAR image visualization, acquired in a descending pass	49
37	Sentinel-1 SAR image read from Matlab	49
38	Segment Dimensions. The result will be segments of 1081x1921 pixels	50
39	CFAR Window formation process	52
40	Standard diagram for Gaussian distribution	54
41	Processing Image delimitation	55
42	Code lines to establish the pixels for each image corner	55
43	Example of the output resulting from the Gaussian CFAR algorithm implementation, $\alpha=6$	56
44	Clustered Image	58
45	K-means with Gaussian CFAR algorithm output	59
46	Input image	60
47	Median smoothing image	60
48	Thresholded image	60
49	Morphological operated image	61
50	Output image	61

List of Abbreviations

Abbreviations	Descriptions
AWGN	Adaptive White Gaussian Noise
BER	Bit Error Rate
DMT	Discrete Multi-tone Modulation
SFNs	Signal Frequency Networks
PDC	Personal Digital Cellular
SDMA	Space Division Multiple Access
BTS	Base Trans-receiver Station
EM	Electra magnetic
GSM	Global System for Mobile communication
VSB	Vestigial Side Band
ICI	Inter-Carrier- Interference
ISI	Inter Symbol Interference
MFNs	Multi-Frequency broadcast Networks
SFNs	Single Frequency broadcast Networks
CSI	Channel State Information
CTF	Space-Time-Frequency coding
WLAN	Warless Local Area Networks
CIRs	Channel Impulse Response

CHAPTER 1

INTRODUCTION

This Chapter is divided into 4 sections: First, a brief description of the purpose of SAR technology, its advantages and its applicability are presented as a kick-off for this report; Second, the formulation of the problem for which it is intended to offer an effective and efficient solution is made; Third, a description of the objectives of the report is presented; Finally, the last section will detail the report structure.

1.1 SAR TECHNOLOGY USE AND APPLICATIONS

The objective of SAR technology is to synthesize an antenna with a larger aperture than the real aperture of the used antenna, i.e., SAR synthesizes an aperture of a much bigger antenna with the use of a smaller one (Owens, Marcelin, & Hunt, 1997). The antenna is carried by a moving platform, which can be, for example, an airplane or a satellite, where throughout its trajectory it processes the signals that are transmitted, forming a bigger aperture, a synthetic aperture, capable of providing high-resolution images despite any weather conditions (Oliver & Quengan, 2004). Giving this potentiality, the development of SAR technology continues increasing nowadays.

For the last few years, the use of SAR technology has been increasing exponentially. SAR data has been used for several applications not only for land recognition and monitoring such as monitoring agriculture cultures, flood mapping, soil moisture, forestry, terrain analysis and geology of surfaces, but also for sea monitoring and activities such as ship detection, illegal fishing, pollution, drug trafficking, sea state, among many others (Moreira, et al., 2013). Because of SAR characteristics, such as offering high resolution images independent of weather conditions and also because it has the ability to cover wide areas of land and sea in a single swipe, satellites use this SAR technique to gather information about any kind of

activity that is occurring on Earth, in order to promote the improvement and innovation of the techniques mentioned before.

Nowadays there are several satellites in orbit with the purpose of supplying information for process and analyze according to the needs at hand. One of the biggest agencies in this sector is the European Space Agency (ESA) which launched several satellites such as ERS-1, ERS-2, Envisat, Sentinel-1, Sentinel-2 and, Sentinel-3 satellites with the purpose of studying and monitoring Earth and its resources and also its structure comprehension and Earth's crust dynamics. The Japan Aerospace Exploration Agency (JAXA) also launched several satellites such as JERS-1, ALOS-1 and, ALOS-2 satellites where its missions are redirected to geological phenomena, land use (agriculture, forestry), observation of coastal regions, geological maps, environment, disaster monitoring, and so on. The Canadian Space Agency (CSA) with Radarsat-1 and Radarsat-2 with the main function of observing Earth to monitor climate changes. There are more agencies and organizations, with their own satellites, focused on the development of numerous applications either in civil or military context such as Japan Aerospace Exploration Agency (JAXA), Deutsches Zentrum für Luft- und Raumfahrt e.V. (DLR), Indian Space Research Organization (ISRO), Italian Space Agency (ASI), National Aeronautics and Space Administration (NASA), Land Remote-Sensing Satellite (LANDSAT), among others.

Furthermore, due to fact that Portugal has one of the biggest exclusive economic zones, with a total of 1,727,408 Km² to monitor and promote safety it's in our navy's best interest to use every tools to complete its missions more effectively with a higher rate of success.

1.2 Problem Statement

Due to the SAR technology applicability and its advantages as well as the dimensions of the maritime area that the Portuguese Navy is responsible to monitor and promote safety, this report intends to offer a solution can be formulated in the following central question (CQ):

CQ: How to provide an expeditious method of detection and analysis of targets along the Portuguese coast in MATLAB using SAR Imaging?

From this major statement arise several derived problems that can be summarized in the following derived questions (DQ):

DQ1: What types of SAR data exists?

DQ2: Where can the SAR images be obtained?

DQ3: What techniques are there to perform this processing?

DQ4: What is the best processing technique for the type of data used?

DQ5: How to validate the results obtained?

To summarize, the problem that this thesis intends to solve is to offer a reliable solution for ships detections in open sea and coastal environment in already focused SAR images by implementing a certain technique.

1.3 Aim And Scope

In order to offer a solution to the problem stated in the previous section, the aim of this report can be summarized as follows:

Implement a detection algorithm using real SAR data from available Sentinel-1, A or B, products, taking into account a basic practical guideline, for all kind of sea environment users, which supports them in the selection of a technique which best suits the task at hands.

To achieve this main goal this report, initially, scopes a brief summary of some the most important SAR historic events, breakthroughs and developments and main SAR characteristics, concepts and principles, then a review of the most used ship detection techniques is made in order to achieve the second part of the main goal, the elaboration of the basic guideline. Secondly, in this report, the chosen technique resulted from the basic guideline in Sentinel-1 SAR images is tested. Finally, the obtained results from the implementation of the chosen technique are validated through a visual analysis and statistical method.

With this main goal, an answer to the central question and its derived questions it's presented, where the initial part of the goal described above will answer to the derived questions 1, 2 and 3, the second part will answer to the derived question

4 and finally the visual analysis and statistical method offer a way to answer the last derived question.

1.4 Report Structure

The goal with the summary of SAR history, concepts, properties and principles, which is done in chapter 2, is to provide essential ground proof that it is a more trustworthy technology and presents better results than the conventional radars, as well as verifying the fact that its development and innovation are constantly made. Then, still in chapter 2, several techniques are described, regarding ship detection where each of them is briefly explained and also, for example, the type of data which is more suitable to implement it, some advantages and disadvantages and finally in what scenario it is more efficient. To complement this analysis, chapter 3 gives a basic guideline to remote sensing researchers, engineers or operational decision-makers for selecting the most suitable ship detection technique for the problem at hand.

Furthermore, a practical example is given by applying the proposed basic guideline to select the most appropriate ship detection technique to the data set available for this report: Sentinel-1 products. The used product type and operational scenarios are described.

In chapter 4, the implemented algorithm for the selected technique (CFAR) is fully described. In chapter 5 the obtained results are analyzed and discussed in a number of different operational scenarios. This is done supported on a visual analysis of the obtained results and by comparing the results gathered by other works that use similar techniques and also the same type of data.

Finally, in chapter 6, a summary of all the work done, as well as a discussion about possible future work and advantages of implementing this line of thinking in our Navy is presented.

CHAPTER 2

STATE OF ART

This chapter presents a summary of SAR technology history, including mission timeline and table of relevant organizations using SAR data and its applications. Then a review of basic SAR concepts and properties is made to help understand the advantages, the benefits and the possibilities that come with the use of this technology. Furthermore, the most applied techniques for Ship detection in the present days are introduced listing its advantages and disadvantages, as well as describing their basic principles.

2.1 Historical Framework and Applicability

Since the invention of the Synthetic Aperture Radar (SAR) in 1951 by Carl A. Wiley, who then made its patenting in 1954 on the United States of America (USA) (Brown & Porcello, 1969), many researches and developments followed the path to improve and innovate this newborn technology which resulted in the launch of the SeaSAT, the first satellite with this technology incorporated, in June 27, 1978.

Figure 1 from “Echoes in Space” course, (ESA EOCollege, 2019), represents the major SAR satellites throughout time where we can highlight those that had the greatest impact on the development of SAR technology:

SeaSAT, launched in 1978, is the first civilian radar of SAR images with an experimental mission of observation of the Earth during 106 days by the National Aeronautics and Space Administration / Jet Propulsion Laboratory (NASA / JPL). This satellite has proven its effectiveness in the collection of oceanic information, obtaining more data than those obtained during 100 years of research onboard ships (E O College - Universitat Jena, 2017).

ERS-1 (European Remote-Sensing Satellite-1) of 1991, was the first satellite of the European Space Agency (ESA) ground observation program, after the end of its useful life and verified its performance and based on the knowledge acquired, **ERS-2** was then launched in 1995 (European Space Agency, 2014).

SIR-C/X-SAR (Shuttle Imaging Radar with Payload C/X-SAR) is the result of a cooperation between NASA/JPL, DARA/DLR (German Aerospace Center) and ASI (*Agenzia Spaziale Italiana*), which developed a radar antenna capable of operating in three different bands (C, L, and X). The hardware system allows the antenna dimensions to be carried aboard the cargo bay of the "Space Shuttle Endeavor" (E O College - Universitat Jena, 2017).

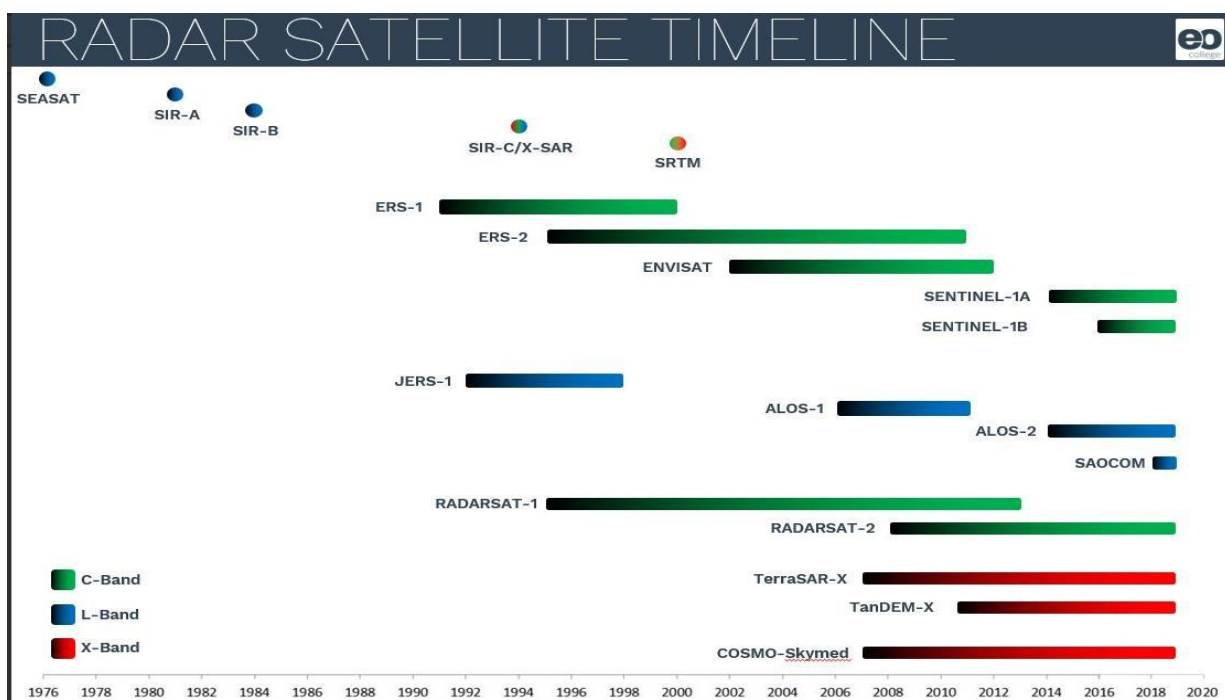


Figure 1 - Major SAR Satellites timeline. Source: "Echoes in Space" course from EO College. (ESA EOCollege, 2019)

Nowadays, the list of countries that study and use SAR Satellites is vast. Among them are Japan, Canada, India, Argentina, North Korean and the 22 members of ESA where Portugal is a member through the Space foundation program for Science and Technology, since November 14, 2000. Due to its continuous developments and shown applicability, the interest and use of SAR technology have become more and more required, and because of that, several companies, summarized in table 1, are responsible to gather the information collected from their satellites, and then share it

with other countries around the world. Table 1 also summarizes the type of mission that each organization is focused on.

Organization	Satellites	Mission Type
European Space Agency (ESA)	ERS-1, ERS-2, Envisat, Sentinel-1, Sentinel-2, Sentinel-3.	Earth Monitoring, Resources management, and monitor.
Japan Aerospace Exploration Agency (JAXA)	JERS-1; ALOS-1; ALOS-2	Apps regarding: survey of geological phenomena, land use, geological mapping, catastrophes monitor.
Canadian Space Agency (CSA)	Radarsat-1, Radarsat-2, Radarsat constellation	monitor the environmental change and the Earth's natural resources in the microwave region.
<i>Deutsches Zentrum für Luft-und Raumfahrt e.V. (DLR)</i>	TerraSAR-X, TanDEM-X;	Apps such as hydrology, geology, climatology, oceanography cartography, etc.
Indian Space Research Organization (ISRO):	RISAT-1, NISAR (com NASA)	Use SAR observation capability for apps like agriculture, soil humidity, marine ice, coast monitor,

		floods monitor, etc.
Comision Nacional deActividades Espaciales	SAOCOM	Management of emergencies or natural disasters and monitoring of natural resources.
Italian Space Agency (ASI)	COSMO-Skymed	Observation and exploitation of military and civil community data (institutional, commercial).
Instituto Nacional de TécnicaAeroespacial (INTA)	PAZ	Earth observation for defense and security purposes.
Korea Aerospace ResearchInstitute (KARI)	KOMPSat-5	Image supply for apps of geological information andmonitor environmental disasters.
National Aeronautics and Space Administration(NASA)	NISAR (com ISRO)	Optimized to measure subtle Earth surface changes associated with crust movements and ice surfaces.

Table 1 - Sums of the Organizations, its Satellites and its Missions. Adapted from UNAVACO,2018. Source: *(Goulão, 2018)*.

As for its applicability, in military or civil context, table 1, it's shows a great diversity of ways to use the obtained SAR information.

SAR technology, like other remote sensing systems, can be installed on both aerial and space platforms, airborne and spaceborne, respectively (Lacomme, Hardange, Masrchas, & Normant, 2001). Both present advantages and disadvantages while comparing with one another. Airborne systems have the advantage of being more flexible in their ability to relocate and capture data anywhere in the world at any time since the space-borne data collection geometry and timetable are limited by the pattern of the satellite orbit. However, they have the disadvantage of being influenced by variations of speed, movements of the aircraft and adverse atmospheric conditions, lacking additional equipment of navigation and correction of the movements. On the other hand, as an advantage, spaceborne systems are not affected by sudden movements, presenting very stable orbits, requiring geometric correction only for the effects of rotation and the Earth's curvature, and the advantage of being able to capture images faster, in a larger area and with more consistent viewing geometry (Lacomme, Hardange, Masrchas, & Normant, 2001).

Changing focus now to civilian applicability, a very good example for this is the information collected by Sentinel-1, Sentinel-2, and Sentinel-3, on the Copernicus program, which is available to the public, free access and without any associated costs (ESA Copernicus, 2019). It becomes a great utility for maritime surveillance, such as monitoring and warnings about ships, water levels, water pollution and the detection of routes suitable for breaking the ice, identifying the best safe passage areas essential to navigation, among many others.

The Echoes in Space course (E O College - Universitat Jena, 2017) divides civilian applications in three wide areas:

1. Terrestrial observation and continuous observation techniques;
2. Maritime observation and related activities;
3. Impact on environmental disasters.

It is important to mention that all this is possible due to not only because of the unique advantage that SAR offers which is the possibility to operate during day and night, as well as being independent of atmospheric conditions, but also because some

satellites have capacity to emit at different wavelengths, usually between bands¹ X, L, C or P, which present different levels of penetration in the materials (E O College - Universitat Jena, 2017).

¹ Radar Bands: P band [0.25 - 0.5GHz/ 60 – 120cm]; L band [0.5 - 1.5GHz/ 20 - 60cm]; Cband [4 - 8GHz/ 3.75 – 7.5cm]; X band [8 – 12GHz/ 2.5 - 3.75cm]).

The possibility of using other SAR techniques such as polarimetry, which allows images with characteristics of color, aspect, roughness, patterns and radiometric intensity to be obtained, allows different information on vegetation types, respective volumes and forest health, mapping, calculating lost and reset quantities, support age of forest support, and biomass derivation, crucial for understanding the carbon cycle, essential to climate stability, enabling monitoring. In short, SAR technology allows mapping under terrestrial biomass, glacier movements, ionosphere, terrestrial topography under large vegetation and subsurface geology. In urban areas, this technology allows monitoring the extension, structure, and growth of cities, identifying and quantifying the present objects (roads, buildings or urban vegetation), making it possible to create 3D digital surface models that are very important for planning, better planning practices. These are only a few examples of applications in the civil environment. There are countless others referred on “Applications of Satellite Imaging Radar”, (M.R. Inggs, s.d.), and on “Synthetic Aperture Radar (SAR): Principles and Applications”, (Alberto Moreira - German Aerospace Center (DLR)).

Now looking to the military field, SAR technology because of its characteristics and advantages, such as high-quality images, independence of weather conditions and the ability to provide information whether on daylight or in his absence, is used in several military mission’s scenarios.

Regarding the military context, several examples can be given, like the role of this technology for Earth mapping on “U.S. Department of Defense’s space-based radar programs”, the NASA ongoing developments such as mapping of other planets, Intelligence, Surveillance and recognition programs in battlefield scenarios, among others (Mchale, 2016). Aircraft and ships around the world already have this technology onboard and it has proven to be effective by accomplishing the goals of their missions. Examples such as the F-22 which is considered the best “air-to-air”

platform capable of pursuing targets in a square mile range, target focusing and photography and be weather independence, the Boeing P-8 Poseidon with a “APY multi-mode synthetic aperture radar”, (Military-Today, 2018) (Keller, Army orders 20 MQ-1C Gray Eagle attack and reconnaissance UAVs and control stations, 2017), among many others practical examples. SAR technology is constantly originating new activities and new technologic developments, and mention all of them would be impossible. However it is possible to stay up-to-date on new upcoming technologies or innovations in this field, because there are countless magazines and journal such as “Military and Aerospace Electronics”, (MILITARY & AEROSPACE ELECTRONICS, 2019), *Air & Cosmos*, (Cochennec, 2019), *Air and Space Power Journal*, (Air and Space Power Journal, 2019), among many others.

2.2 Basic Concepts And SAR Properties

To comprehend why this technique is now widely used and a growing interest in new developments and innovations, it's important to understand how it works. For this purpose, in this subchapter, it will be made a review of some of its fundamental concepts and properties, in order to make it easier to understand its advantages and benefits. Since SAR theory is a complex and dense topic, it's important to highlight that the next sections will only give sufficient knowledge to how this technique works.

Starting from the beginning by defining what is a SAR. A Synthetic Aperture Radar (SAR) is, accordingly to National Aeronautics Space Administration, Earth Observatory glossary, “A high-resolution ground-mapping technique that effectively synthesizes a large receiving antenna by processing the phase of the reflected radar return. The along-track resolution is obtained by timing the radar return (time-gating) as for ordinary radar. The cross-track (azimuthal) resolution is obtained by processing the Doppler phase of the radar return. The cross-track 'dimension' of the antenna is a function of the length of time over which the Doppler phase is collected”. Or, accordingly to radartutorial.eu, radar basis, “a coherent mostly airborne or space-borne side-looking radar system which utilizes the flight path of the platform to simulate an extremely large antenna or aperture electronically, and that generates high-resolution remote sensing imagery. Over time, individual transmit/receive cycles

(PRT's) are completed with the data from each cycle being stored electronically. The signal processing uses magnitude and phase of the received signals over successive pulses from elements of a synthetic aperture. After a given number of cycles, the stored data is recombined (taking into account the Doppler effects inherent in the different transmitter to target geometry in each succeeding cycle) to create a high-resolution image of the terrain being overflown.”(radartutorial.eu). In lighter terms, it’s a smaller radar that through a moving platform has the ability to create high resolutions images that can cover big areas of earth land or sea. To comprehend how this is possible it is required to understand the principles associated with this technique, thus a quick review is in order.

2.3 SAR Systems Radar Equation

For any conventional radar, its purpose is to detect targets and estimate its parameters through the emission of an electromagnetic signal and reception of corresponding echoes. Figure 2 illustrates the operating principle of conventional radars.

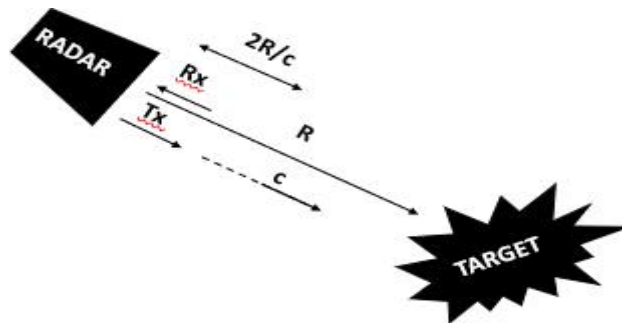


Figure 2 - Tx/Rx of a satellite. c =light speed; R = distance to target.

It’s through the Conventional Radar Equation (1) that the SAR equation (2) is deduced. By understanding the Tx/Rx process using only one antenna, which is represented in fig. 3, the Conventional Radar Equation, as deduced in many literature works, like (ESA - Earth Online, 2018), can be written as a function of the received power, P_r , as follows:

$$P_r = \frac{P_t G^2 \sigma \lambda^2}{(4\pi)^3 D^4}$$

P_r = Received Power
 P_t = Transmit Power
 G = Antenna Gain
 σ = Radar Cross Section
 λ = Transmit Wavelength
 D = Distance

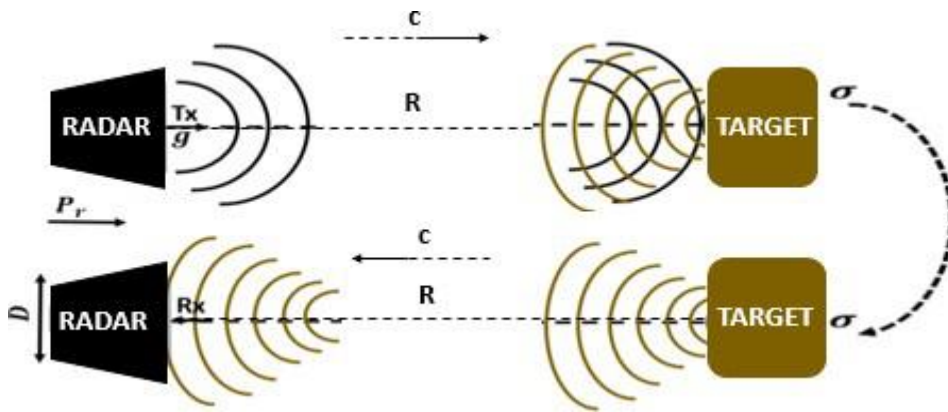


Figure 3 – Illustration of the Tx/Rx process of a radar signal.

Where P_t represents the transmission power, P_r the received power, σ the target Radar Cross Section, R the distance to the target, D the antenna real aperture and g the gain of the antenna. In short, the radar transmits a signal with a certain transmission power, P_t , and gain, g , which then travels a distance R , accordingly to a spherical model, respecting the factor $[1/4 \cdot \pi \cdot (R^2)]$, until it reaches the target, then part of the signal is reflected and received by the radar with a certain received power, P_r , traveling at the same speed (c).

What makes SAR equation (2) different from the equation (1) is that it's based on the SAR scan process where successive signals are transmitted and received, in addition to the process of a conventional radar, i.e., the received power per pulse necessary to take into account the number of pulses in the time corresponding to the synthetic aperture, N_A , and the pulse time, T_p , resulting as follows (Goulão, 2018):

$$\text{SAR Radar Equation: } P_{rSAR} = P_r * N_A * T_p = \frac{P_t * T_p * PRF}{(4\pi)^3 R^3 V_L} \frac{g^2 \lambda^5}{\sigma} .$$

2.4 SAR Geometry and Acquisition

For a better understanding of SAR theory, figure 4 illustrates a Strip Map geometry, which will be explained *a posteriori*, for geometry acquisition.

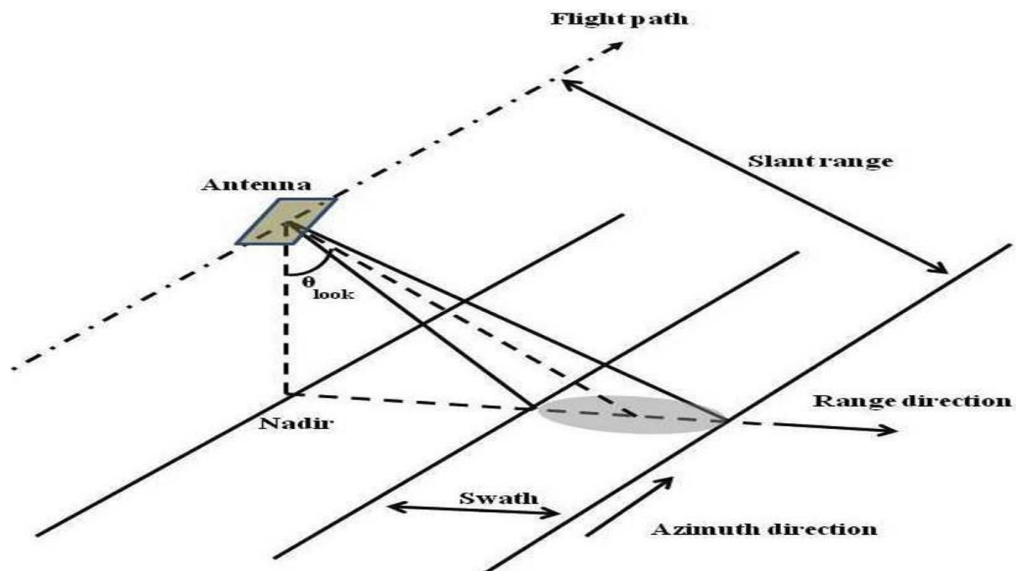


Figure 4- SAR Strip Map geometry. Source: (NASA, 2018)

Through figure 4 it becomes clear how the synthetic aperture is made. Since the radar is carried along the flight path trajectory through time, the footprint changes and that's how the simulation of a larger antenna is made, because the system will process all the collected information. Figure 5 illustrates how this processing is made.

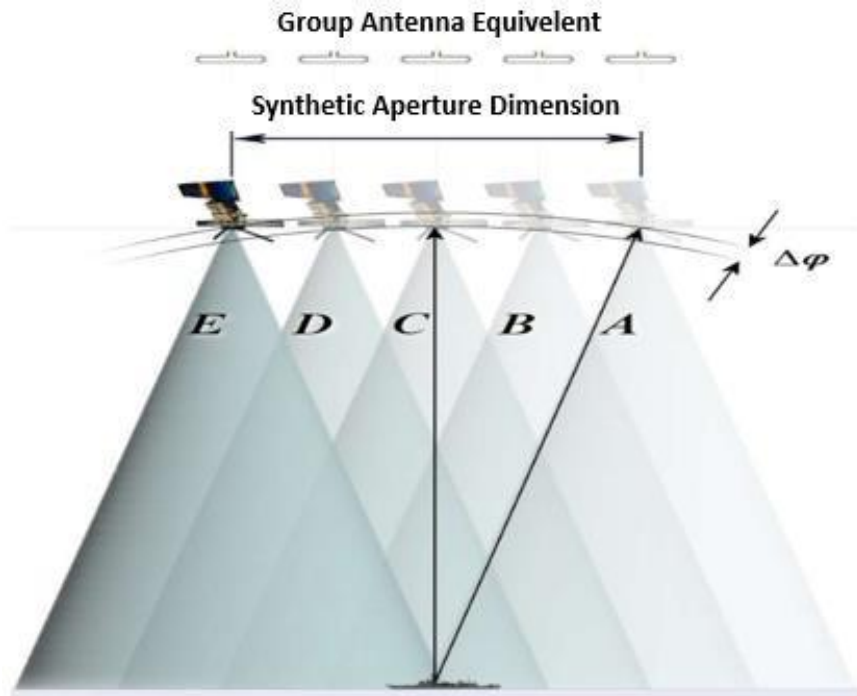


Figure 5 - Simulation of a Synthetic Aperture. Source: (Wolff, 1983)

In figure 5, where A, B, C, D, and E represent the real aperture of the antenna and then after gathering all information through time it simulates a larger antenna with the combination of each real aperture due to the satellite movement, the synthetic aperture.

The interest of simulating a larger antenna is the resolution improvement, i.e. the larger the antenna aperture, the smaller the resolution beam, given the expression:

$$\Delta_{AR} = R\alpha = \frac{R\lambda}{D}, \quad (3)$$

where R = range and $\alpha = \frac{\lambda}{D}$ = diffraction angle (λ = wave-length and D = antenna physical aperture).

For satellite data acquisition there is a wide diversity associated geometries, such as StriMap (SM); interferometric SAR (InSAR), Spotlight, Inverse SAR (ISAR), SCANSAR, among others (P.Marques, 2016).

For SM, represented in figure 6, the antenna illuminates a strip of terrain and collects data continuously with a fixed nadir angle and azimuth angle. In the case of SENTINEL-1, for example, the SM mode acquires data with a visible bandwidth of 80Km and a resolution of 5m by 5m.

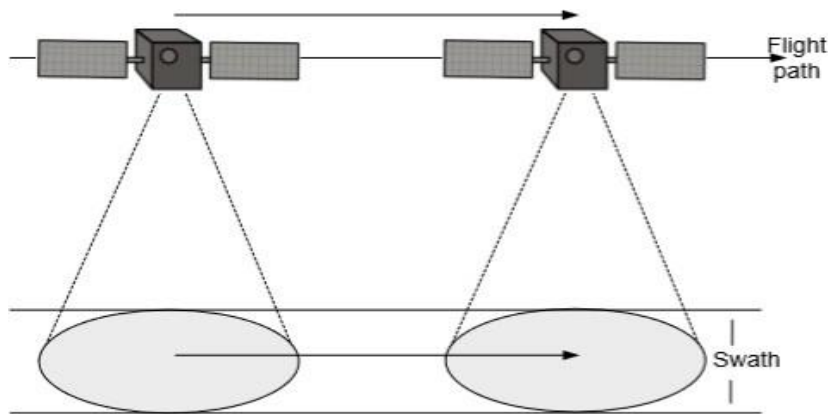


Figure 6 - StripMap mode (SM). Source: (P.Marques, 2016).

In the Case of InSAR, in figure 7, a pair, or more, of coherent phase from SAR signals are combined in order to provide three-dimensional information about Earth's surface (PCI Geomatics, 2018). These coherent phases are taken from slightly different sensor positions or from two SAR signals from very similar viewing geometries of the region under observation, i.e., they can be acquired from the same satellite or two satellites that cover and have similar orbits. It's by comparing these phases that is possible to determine the elevation and measurements of surface deformations of the terrain. This geometry has several applications such as geophysical monitoring of natural hazards: earthquakes, volcanoes and landslides, glacier motion analysis, digital elevation mapping, among others (ESA, 2018).

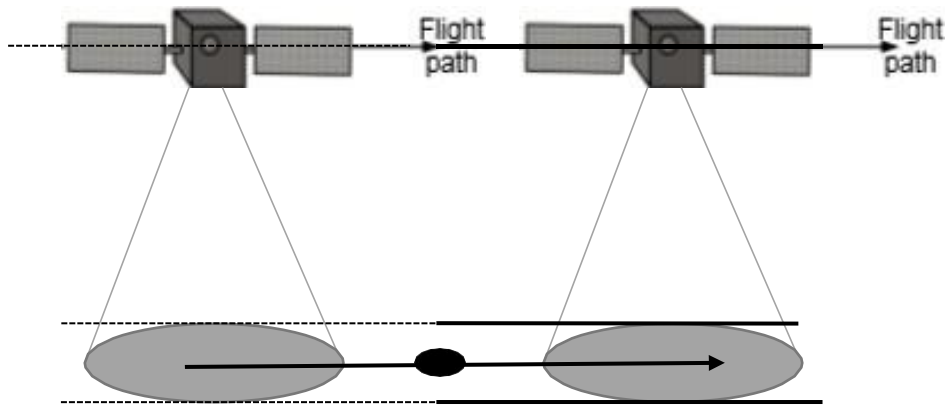


Figure 7- InSAR mode.

In Spotlight mode, illustrated in figure 8, where the radar has an antenna capable of changing its position, either mechanically or electronically, to illuminate a region of interest for a longer period of time thus synthesizing a larger antenna. In this sense, since the system detects the target much earlier and fails to see it much later, the phase excursion will increase and the resolution increases accordingly. Note that the aperture is as large as the time we are illuminating, so the limit is our mechanical or electronic capability and once again, the topography of the terrain also imposes limitations. This geometry is used when the goal is to obtain a higher resolution of a specific area (Marques P. , High resolution SAR imaging and signal processing, 2016).

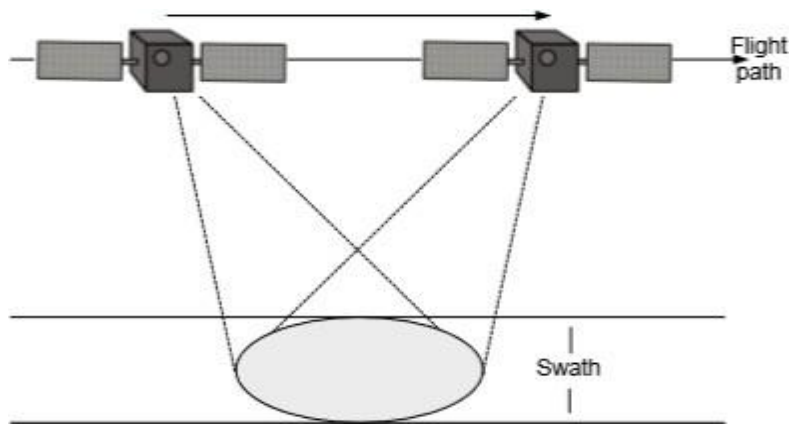


Figure 8- Spotlight mode. Source: (P.Marques, 2016).

Figure 9 represents the ISAR mode, where in this situation, the high-resolution images are extracted from a static antenna and the detection is done by moving the target relative to the antenna, processing the data coherently.

This geometry has military relevance since it is used to obtain high-resolution images of the target, i.e., it is of interest, for example, the identification of vessels in marine monitoring actions.

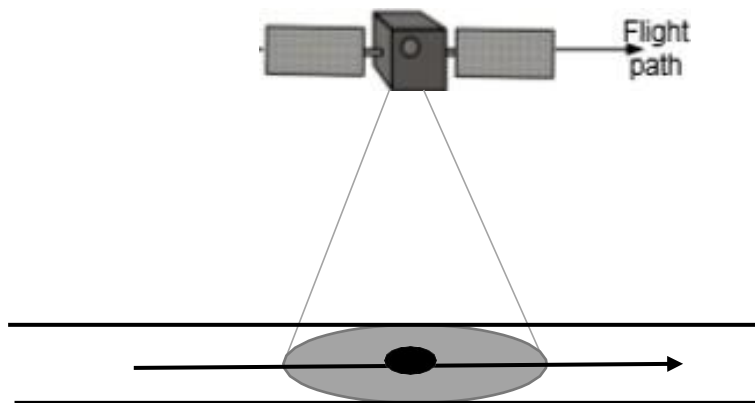


Figure 9 - ISAR mode (P.Marques, 2016).

Finally, the SCANSAR mode, represented in figure 10, provides a wider swath, i.e., it obtains a larger footprint, larger than the spotlight and strip map mode, by changing the illumination angle and rejoin the sub-swath images together during the data acquisition timeframe. In this case, the resolution in azimuth is degraded due

to the non-continuous illumination of the terrain, when comparing to the strip map acquisition.

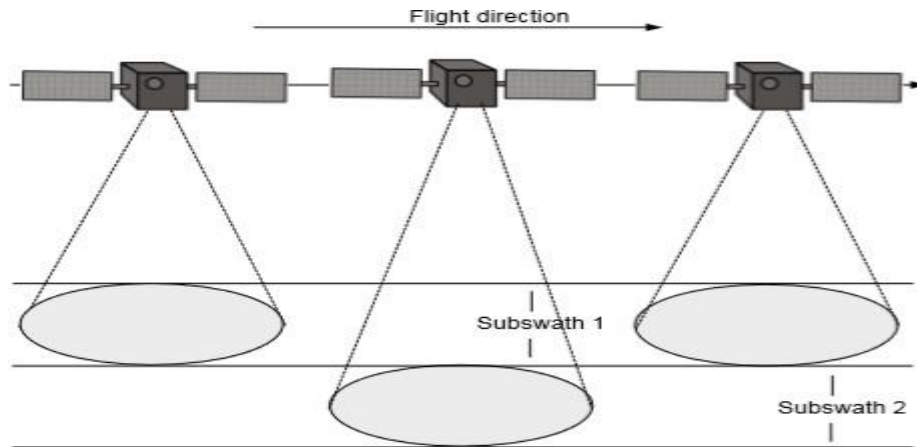


Figure 10- SCANSAR mode. Source: (P.Marques, 2016).

2.5 SAR Processing and Factors that affect Its Image

SAR basic image formation consists of two steps which are independent of the order they are done, i.e., they are commutative. One is Range Compression and the other one is Azimuth Compression. Combining the results of these two compressions, SAR raw Data originates a SAR image. Despite SAR images can have high resolution in order to be well interpreted, there are some factors which can lead to a not so accurate interpretation and also affects its quality in terms of resolution. Factors like the Range Cell Migration (RCM) which can cause blurring in the output image due to the data dispersion on the matrix caused by the variation of the distance between the radar and the target. Other is speckle which is an unavoidable noise that degrades the SAR image quality due to the surfaces of the materials that represent a spike on the wavelength scale. And a simple moving target can lead to an inaccurate interpretation because the target will be misplaced on the image (doppler effect).

But other factors must be mentioned as well, like Lifting Displacement, Foreshortening, Layover and Radar Shadow effect (ESA - Earth Online, 2018).

2.6 Ships Detection

After reviewing some of Radar history events and its applicability as well as its basic concepts and SAR properties with a focus on making it easier to understand the fundamental aspects of its theory as well as making it more perceptible why this technique is so promising and effective, comes the subject Ship detection. The purpose of this topic has two major reasons. On one hand it's because of the market opportunities since ESA release Sentinel-1 and Sentinel-2 data for the public use, which means access to a constant source of data to work with and on the other hand, since this is a Naval Military report and Portugal has ones of the largest sea areas at its responsibility, not only to promote and provide navigation safety but also to keep a constant and accurate monitoring of the area. So, for this reason, it seems fit to provide a good base of knowledge in this area by going through the most used techniques for ship detection or oils spills, for example.

As mentioned previously, several techniques have been studied, implemented and improved to enhance automatic ships detection using SAR images (F. Quina, 2019). Depending on how the information is gathered and processed each technique presents different performances and results. Nowadays there are several operational missions underway and the need to acquire better results in ships detection, oil-spill detection or any kind of sea activity monitoring, such as illegal fishing, pollution or drug trafficking, is fundamental to preserve and promote navigation safety as well as constant and accurate monitoring of the surroundings.

In regard to ship detection, either at open sea, near the coast, or in harbor, there are several studies made, such as newly proposed models or just simple demonstrations and study of techniques already known. The next sections will summarize some of the most used and well-established ship detections techniques which are multi-look imaging techniques, Constant False Alarm Rate (CFAR) based techniques, polarization techniques, and amplitude change detections (ACD) techniques. It will be made a brief summary of its principles and characteristics with studies already carried out. Furthermore, Annex 2 presents an article that was produced and present in the Oceans 2019 conference that took place in Marseille about this Ship detection techniques review as well as the elaboration of the Basis Guideline in chapter 3.

2.7 Multi-look Imaging techniques

This technique is characterized for being able to reduce the speckle at the expense of system resolution, by incoherently adding two or more statistically uncorrelated speckle patterns (Ouchi, 1985).

First, a full synthetic aperture is divided into two or more sub-apertures or “looks” in either time or frequency domain through which the corresponded sub-images are formed and summed on an intensity basis to produce a single final image (Ouchi, 1985). With this technique, stationary targets are correctly imaged, but regarding to moving targets, the scenario is different because the position of the moving targets changes between looks.

SAR multi-look processing principle for static and moving targets is well-known, and it is briefly explained in several publications like (Ouchi, 1985) and (R.K. Raney, 1971). Let us consider a random point, with coordinates x and y in ground azimuth and range direction, respectively, and if the transmitted pulse is linearly frequency modulated (FM), the return signal has the following standard form (Ouchi, 1985):

$$E(t, r, x, y) = E_0 \cdot e^{i\omega(c-\frac{zr}{c})} \cdot e^{-\frac{\pi\alpha}{2} \left(\frac{2r}{c}\right)^2},$$

where r is the slant range distance radar/target, which is given by:

$$r^2 = (R + y \sin\theta)^2 + (Vt - x)^2,$$

Where E_0 represents the scattering amplitude, the pulse envelope and de the far- field beam pattern of the target, ω is the pulse center frequency, α is the linear FM rate, V and c the platform radar and radio wave velocities, respectively, θ is the radar look angle, R the reference slant range distance radar/target, t is the azimuthrange time variable which is discrete but can be treated as continuous by providing an appropriate pulse repetition frequency to satisfy the sampling theorem and r is the slant range time variable. Figure 11 is the SAR geometry to help understanding its mechanism.

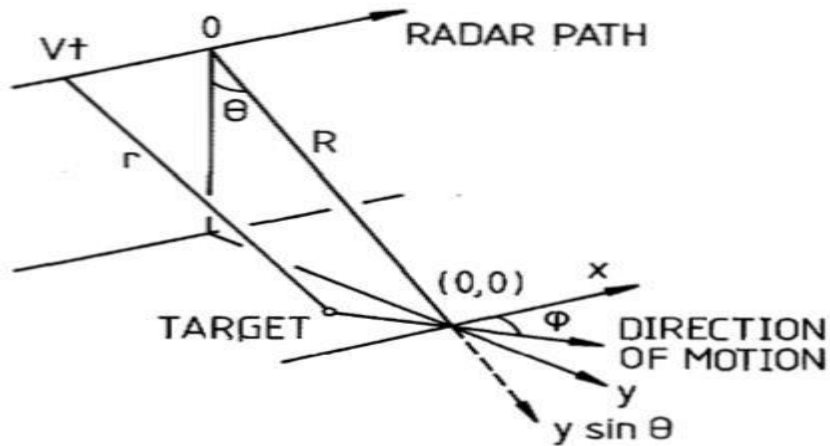


Figure 11 - SAR Geometry. Source: (Ouchi, 1985).

The basic principle of this process in splitting the synthetic aperture into looks, i.e., the radar will travel a certain path in a determined period of time, from that it is acquired a synthetic aperture which it will then be divided into sub-apertures in time, the so-called looks. Each look gives different information about the targets that are being observed because these sub-apertures are synthesized at different times. It is possible to distinguish between stationary and moving targets and potentially estimate their velocities. Giving a visual of the split process figure 12 demonstrates how it's done.

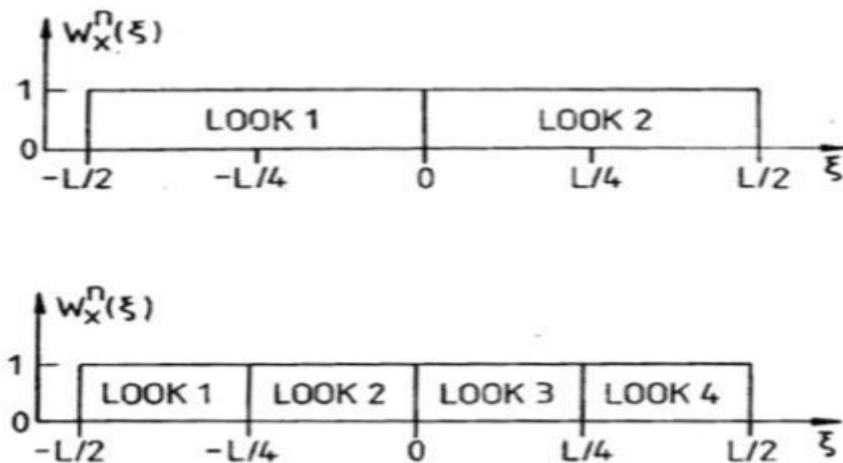


Figure 12 - Synthetic aperture split process. Source: (Ouchi, 1985). where N is the total of looks, $L = V/T$ is the full synthetic aperture length and W_n is the rectangular window of look n .

For moving targets, the principle is the same but the equation (5) is rewritten by (Ouchi, 1985):

$$r^2 = (R + v_r t)^2 + (V - v_x)^2 t^2,$$

where V_r and V_x are the slant range and azimuth velocity components, respectively.

Figure 13 demonstrates how the process of a moving target in the range direction, where Y_n are where the radar sees the moving object along its trajectory, i.e., through time, and T_n are the sub-looks.

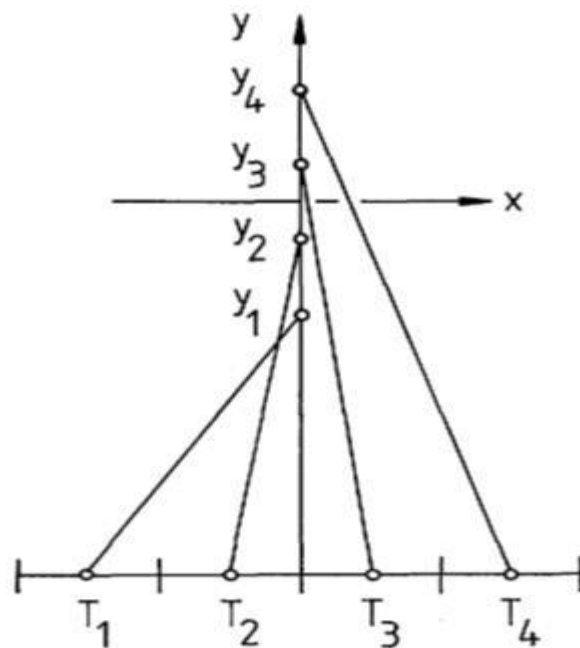


Figure 13 - Detection of a moving target. Source: (Ouchi, 1985).

In (Ouchi, Tamaki, Yaguchi, & Iehara, 2004), a technique based on coherence images derived from its cross-correlation in RADARSAT-1 data is tested. This method produces a coherence image by cross-correlating two small images extracted by moving windows from multi-look images (Ouchi, Tamaki, Yaguchi, & Iehara, 2004), i.e., it grabs two sequential “looks” of a multi-look image and originates an image based on the similarities and non-similarities of those two “looks”. The detection of ships is possible because of the higher coherence between the “looks” for

ships than for the sea, which it's easily explained by saying that the sea changes between looks and the ships have always the same form. For this study case, the results were quite reasonable, it was possible to detect the majority of the ships present in the region under study. The following images represent and summarize the studied area and its features and also some conclusions about the obtained results.

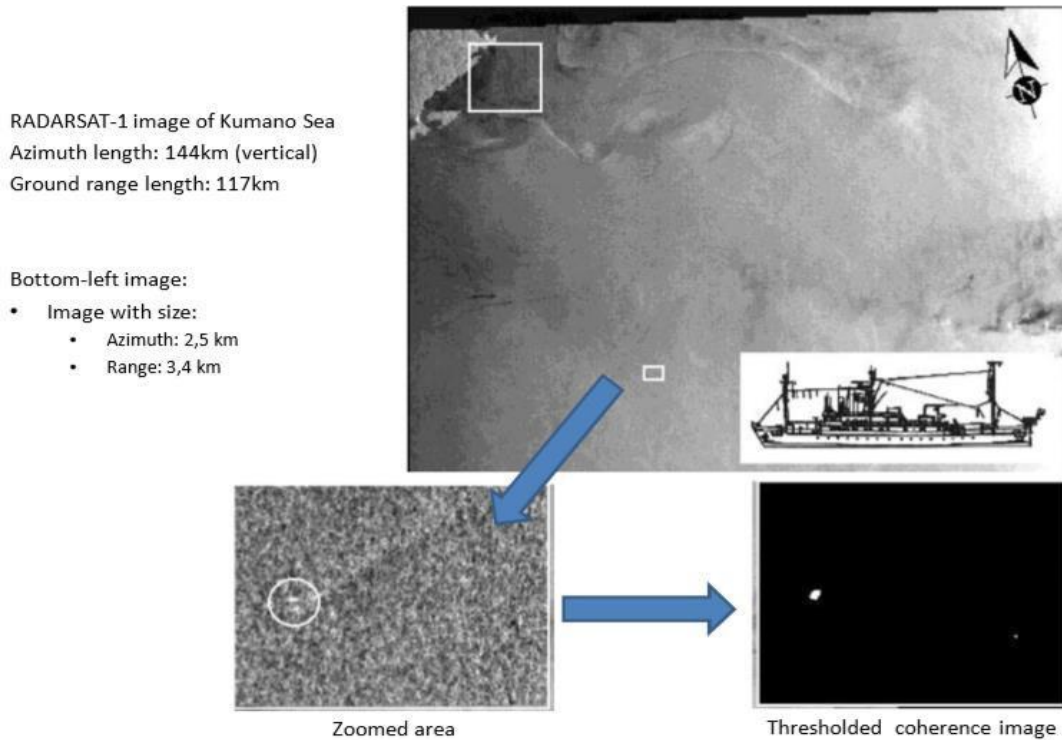


Figure 14 - RADARSAT-1 dataset visualization and specs.

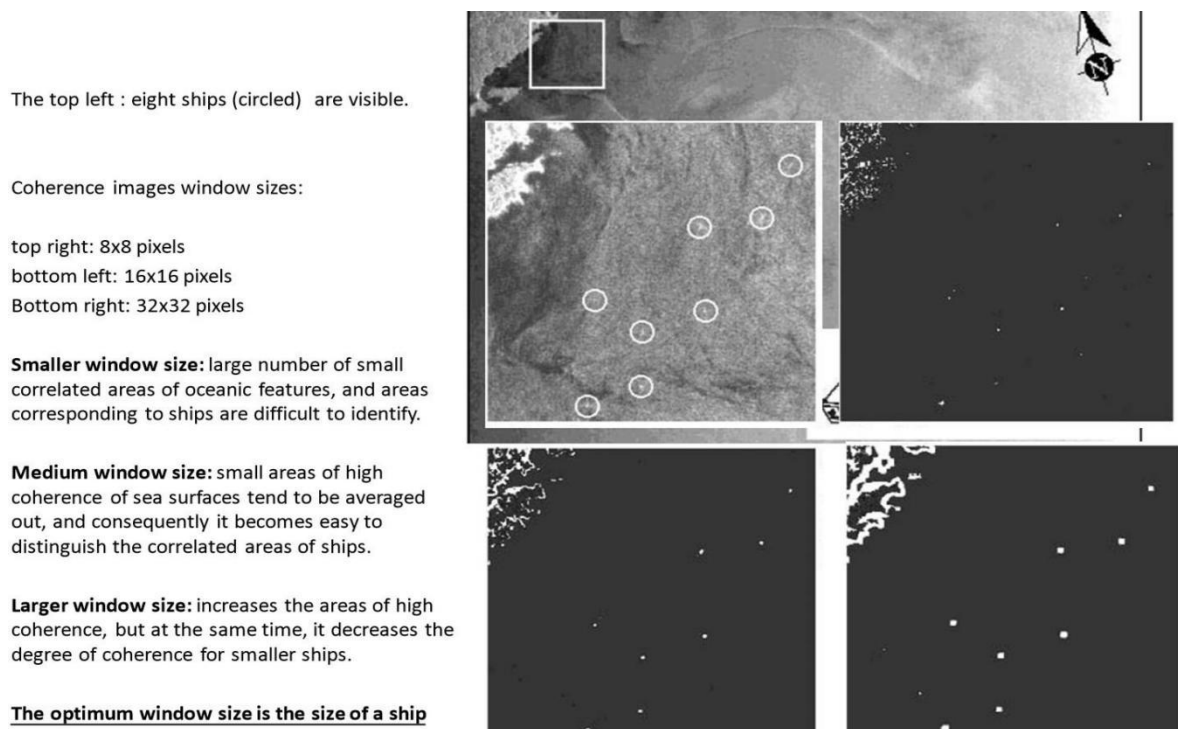


Figure 15 - Results obtained and explanation of the use different windows.

Another example is the application of Multi-look processing on THz SAR systems to detect moving targets mentioned in (Wuhan, Xia, Liu, & Center, 2018). Here the problem of the slowly moving targets is solved due to the characteristics of THz SAR systems in comparison with the X-band SAR systems. The results obtained in this study show that an algorithm using multi-look processing could provide good results.

2.8 Constant False Alarm Rate techniques

Constant False Alarm Rate (CFAR) based technique is the most used technique to detect ships. CFAR is an adaptive algorithm used in radar systems. Generally speaking, it finds a threshold to establish if there's a ship or not in the analyzed area. This threshold is computed through the background clutter, noise or interference analysis. In its simplest form, the algorithm is a simple clutter adaptive statistic that outputs a CFAR when the background clutter is of a Gaussian distribution (Liao, Wang, Wang, & Jiang, 2008). But the Gaussian distribution is only appropriate if a large number of samples have been average (Liao, Wang, Wang, & Jiang, 2008), so in order to get a better output in terms of accuracy and effectiveness, it's necessary to

determine what is the best suitable probability density function(pdf) that can model the background clutter, noise or interference.

Ship detection from sea clutter is an example of the implementation of a CFAR technique that uses an alpha-stable distribution to best identify slowly moving or nearly stationary targets, (Liao, Wang, Wang, & Jiang, 2008). Here, instead of using the ship's wake for ship detection, it uses the difference of the radar cross-section (RCS) of a ship from the sea clutter, with an appropriate threshold. This turns out to be effective because the RCS of ships is higher than the sea clutter due to the ships structure and metallic composition which results on multiple reflections (Liao, Wang, Wang, & Jiang, 2008). Regardless of the good performance of the conventional CFAR, using a gaussian distribution, other pdf can also be used to obtain reasonable results such as Weibull or K-distributions. But each of these distributions could sometimes fail to provide a reasonable fit to the amplitude statistics of the clutter and there is where it comes in the alpha-stable distribution which, accordingly to (Liao, Wang, Wang, & Jiang, 2008), it has the potential to model well the impulsive spiky signal present in the sea clutter.

To visually demonstrate the better performance of the α -stable distribution, in comparison to others, the next figures presents a zone of the surroundings seas near Hong Kong and the outcome of the algorithms used, where each white dot represents an alarm and the ones that are within a box are the real alarm, i.e., the true ships in the area, the rest are false alarms.

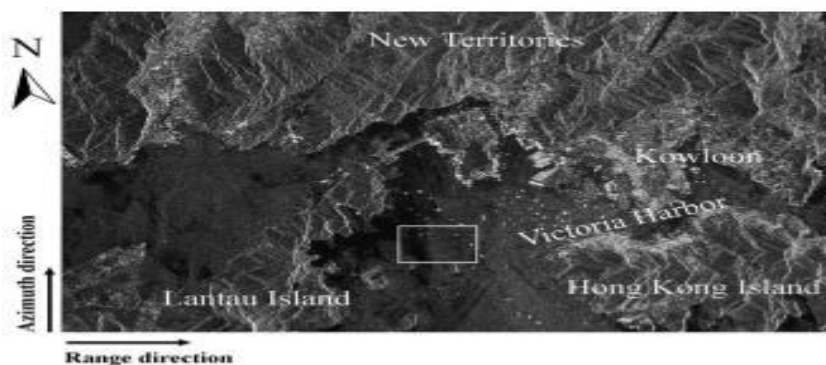


Figure 16 - Target Area for analysis. Source

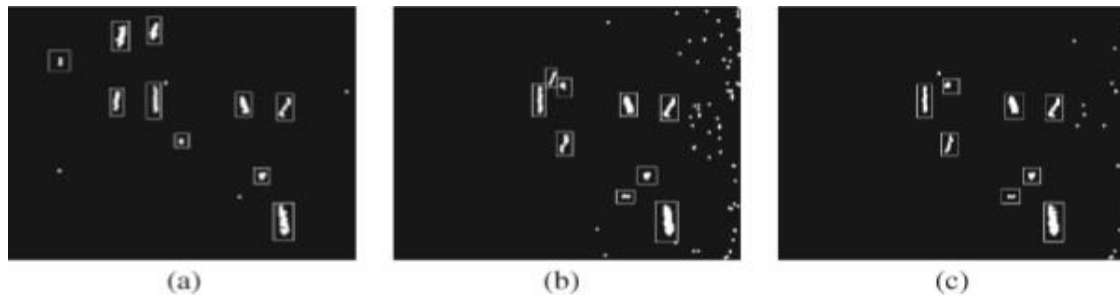


Figure 17 - Ship Detection based on CFAR algorithms. (a) - alpha stable distribution; (b) - Weibull distribution and (c) - K-distribution. Source: (Liao, Wang, Wang, & Jiang, 2008)

Another variation of the CFAR technique is a method that suggests analyzing the sea in two regions, sea region, and buffer region, introduced in (Zhai, Li, & Su, 2016). The approach here is to divide the SAR image into zones: a region with only sea and a region where there are sea and land, i.e., the buffer regions. For sea regions, a variation of a CFAR is used, the truncated statistics CFAR (TS-CFAR), which can provide accurate background clutter modeling and fine detection performance in high-target-density situations (Liao, Wang, Wang, & Jiang, 2008). For the buffer regions are used a technique based on saliency detection because the CFAR has difficulties regarding the inshore ship detection (Liao, Wang, Wang, & Jiang, 2008). To a better understanding of this process, figure 18 shows the steps made in this CFAR based novel.

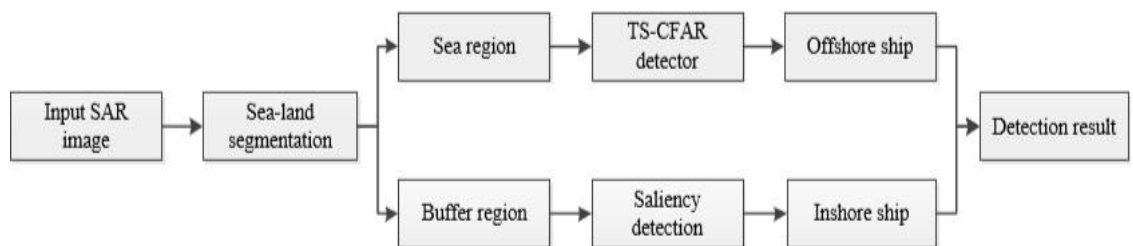


Figure 18 - Block Diagram of Segmentation based CFAR algorithm. Source: (Liao, Wang, Wang, & Jiang, 2008).

Despite some small differences in each method, it's possible to identify that CFAR methods present a very good ship detection whereas it is at sea regions, at land and sea regions and even at harbor regions. For each zone, there is a different approach of the conventional CFAR by adding mathematical weight, which, consequently, will increase the computational processing time, but it will improve the performance of ship detection.

2.9 Polarization techniques

SAR polarimetry or polarization techniques are more redirected not only to the ship detection but also for its characterization and, for example, oil-spill or other human-made structures such as buoys and oil or gas platforms, because measuring the full scattering matrix allows building a powerful observation space sensitive to shape, orientation and dielectric of the scatters (Moreira, et al., 2013). Each set of polarimetric data provides different information about the area of interest. For single channels polarizations (HH, VV, or HV), HH polarization permits the best ship-sea contrast, whereas VV polarization provides more information on sea surface conditions (Vachon, 2004). Although single channels already provide reasonable results in ship detection and characterization, there are other methods that have been already studied such as dual-pol and quad-pol, which combine either two single channels or four, respectively (Reza Shirvany, Marie Chabert and Jean-Yves Tourneret, 2012). It's, for example, through the degree of polarization (DoP) that it's possible to detect and characterize either ships, oil-spills or any other man-made structure in the sea because it helps to determine the nature of the objects that backscatter the electromagnetic field (Reza Shirvany, Marie Chabert and Jean-Yves Tourneret, 2012).

To illustrate the efficiency of this technique the following examples are taken from an article published on the Institute of Electrical and Electronics Engineers (IEEE) with the title "Ship and Oil-Spill Detection Using the Degree of Polarization in Linear and Hybrid/Compact Dual-Pol SAR", (Reza Shirvany, Marie Chabert and Jean-Yves Tourneret, 2012). The following images are regarded to buoys detection where,

in figure 19 and 20, each box represents a different detection mode that has been used and the RADARSAT-2 and google images of the tested area.

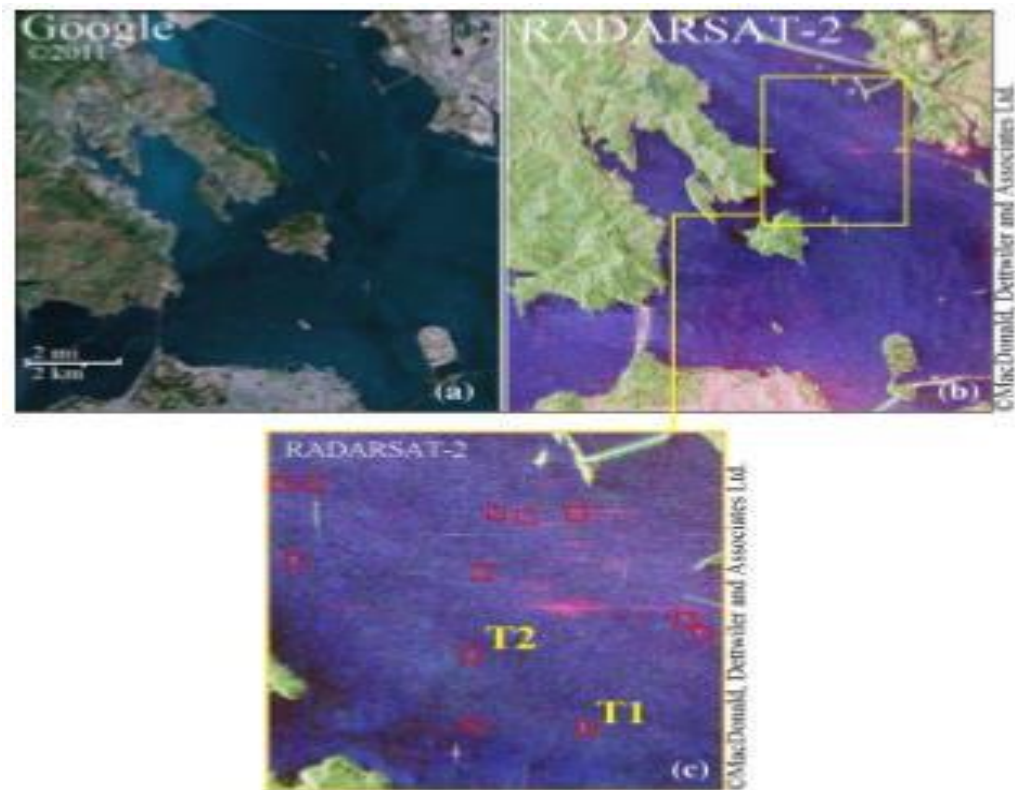


Figure 19 - San Francisco Bay, USA. (a) Google Earth image of the area (b) Pauli RBG image of the RADARSAT-2 fully polarimetric data set. (Reza Shirvany, Marie Chabert and Jean-Yves Tournet, 2012)

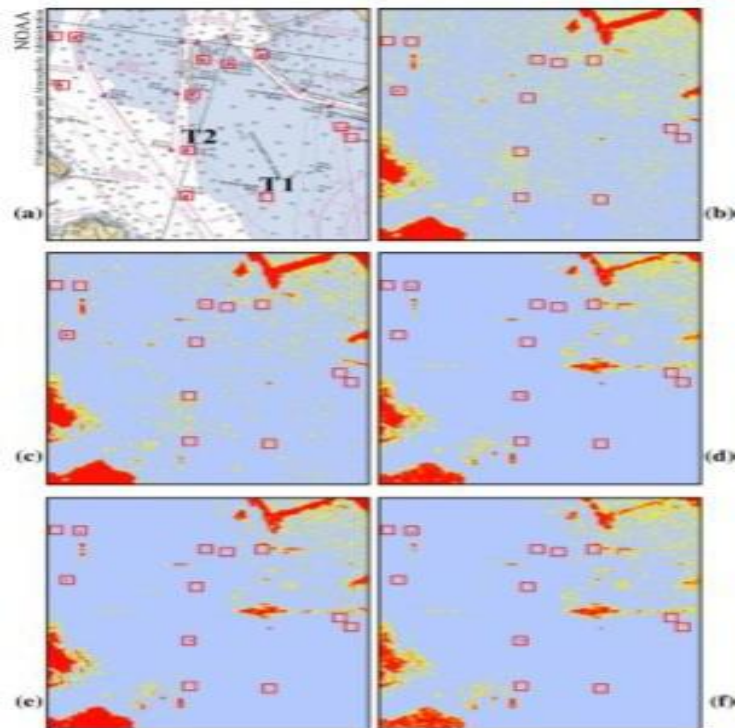


Figure 20 - (a) Nautical chart showing buoys positions. (b) - (f) Maps of the DoP over San Francisco Bay in different hybrid/compact and linear dual-pol modes. (b) HH-HV. (c) VH - VV. (d) HH-VV. (e) CL-pol. (f) $\pi/4$. Source: (Reza Shirvany, Marie Chabert and Jean-Yves Tournet, 2012)

Accordingly to (Reza Shirvany, Marie Chabert and Jean-Yves Tournet, 2012), the hybrid/compact modes, (e) and (f), can easily distinguish the buoys whereas the linear dual-pol modes, (b) and (c), hardly make their detection and identification. Another fact is that the results acquired from HH-VV mode, (d), are very similar to hybrid/compact modes.

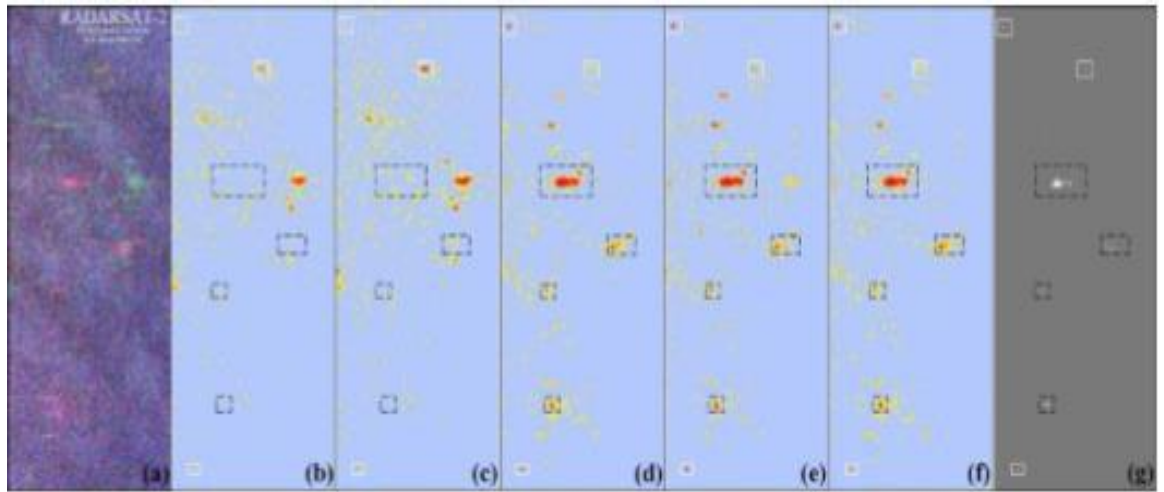


Figure 21 - (a) Pauli RGB image of test area from San Francisco Bay, RADARSAT-2 fully polarimetric data set. (b) - (f) Maps of DoP over the test area in different hybrid/compact and linear dual-pol modes. (b) HH-VV. (c) VH-VV. (d) HH-VV. (e) CL-pol. (e) $\pi/4$. (g) ship Detection results, based on quad-pol data. Source: (Reza Shirvany, Marie Chabert and Jean-Yves Tournet, 2012)

Here in figure 21, it is also clear that hybrid/compact modes [(e) and (f)] detect more clearly the targets. Finally, a further study in this paper on oil-spill and oil-rig, detection and identification, figure 22, also points out that hybrid/compact dual-pol modes show better results. Figure 22 shows the data set used to perform the analysis in figure 23.

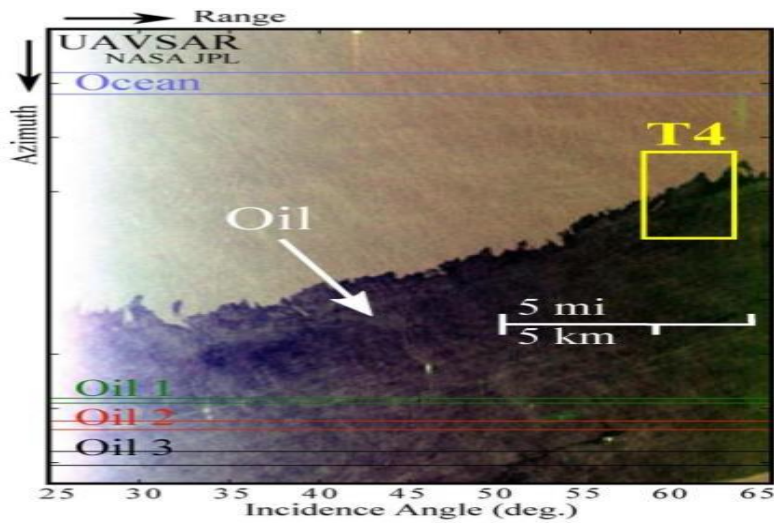


Figure 22 - Pauli RGB image of the NASA/JPL UAVSAR fully polarimetric dataset from the Deep water Horizon oil spill in northern Gulf of Mexico, USA. Source:

(Reza Shirvany, Marie Chabert and Jean-Yves Tourneret, 2012)

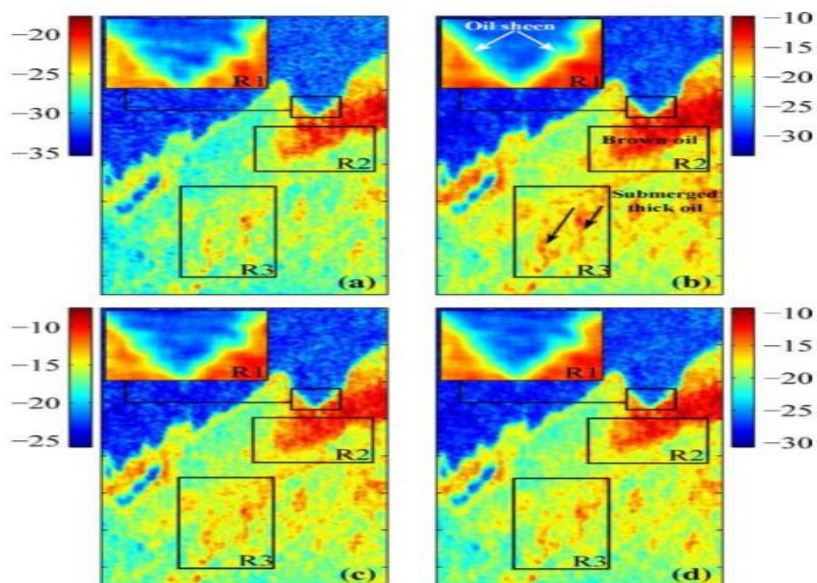


Figure 23 - Oil-slick property/type recognition using the Dop (DB) in dual-polSAR. (a) VH-VV. (b) HH-VV. (c) CL-pol. (d) . The region is a subset of UAVSAR data set. Source: (Reza Shirvany, Marie Chabert and Jean-Yves Tourneret, 2012)

2.10 Amplitude Change Detection techniques

To successfully apply Amplitude Change Detection (ACD) techniques it is required to do a pre-processing of the input imagery to create a registered and

speckle-filtered stack (Sharma, Caves, Greene, & Fernando, 2018). These techniques are best suitable to work with a stack of imagery acquired with the same viewing geometry (i.e. same look and pass direction, incidence angle, and spatial footprint) and same polarization (Sharma, Caves, Greene, & Fernando, 2018), because it's based in amplitude differences between images to identify the possible changes that can occur. One fundamental step in these methods is reducing the speckle because it confuses visual image analysis and generates false alarms during automated change detection (Sharma, Caves, Greene, & Fernando, 2018). To solve this problem and to preserve spatial resolution over point targets and linear features, it's used a combination of spatial and temporal filtering (Lee, 1981). Figure 24 shows the steps of the pre-processing before applying an ACD technique.

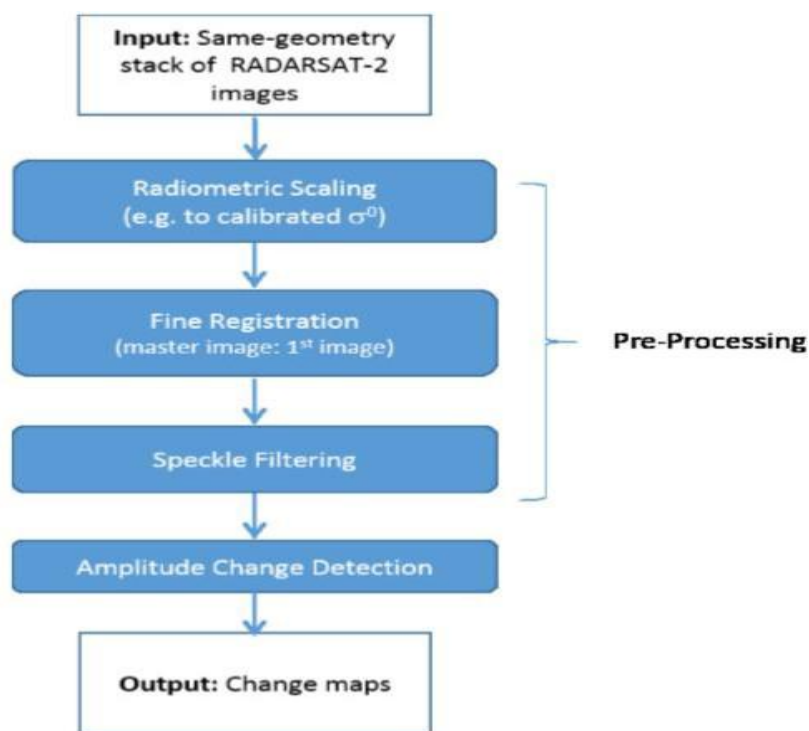


Figure 24 - SAR Amplitude Change Detection processing chain starting from detected input products. Source: (Sharma, Caves, Greene, & Fernando, 2018).

Examples of these ACD techniques are Pairwise and Time-series ACD methods, that basically the first one compares a pair of co-registered SAR images to compute a changing statistic on a pixel by pixel basis and the second one uses a time series of

SAR acquisitions from the same geometry for increased sensitivity to persistent changes (Sharma, Caves, Greene, & Fernando, 2018).

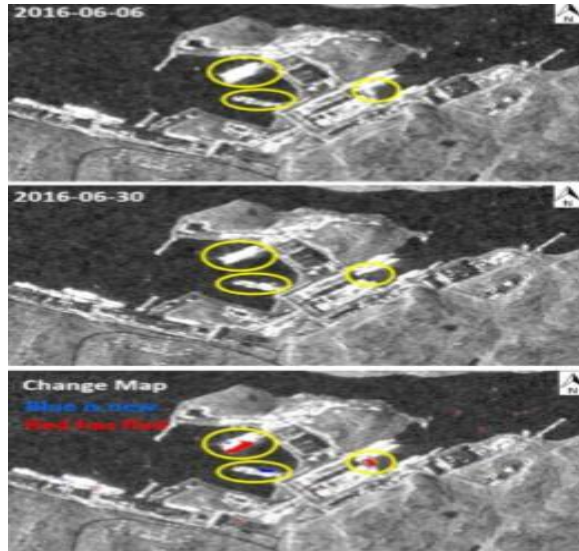


Figure 25 - Pairwise ACD applied to RADARSAT-2 XF data for harbour monitoring near Murmansk. Chip size is +/- 2.3 x 1.3 km. Source: (Sharma, Caves, Greene, & Fernando, 2018).

Figure 25 is an example of the application of Pairwise ACD algorithm, where the first two images show the pre-processed image from the identified days which from their analysis and comparison it's possible to identify the movements that have occurred on the harbor. Blue represents new ships and red represents the ships that leave the harbor. This method, as mentioned before, is the comparison of two images from the same area but with a different timeline in order to produce a third image where changes are clearly visual. A common approach is to identify and detect the changes present on the images is using a probabilistic model where the outcome results are based on the differences between images, which normally are measured through the equation (13), the Amplitude Ratio (AR) in decibel(Db), where I_1 and I_2 are the intensities. If its value is positive indicates an increase of the backscatter and if its negative indicates a decrease in the backscatter, thus it is possible to know whether a target appeared or disappeared (Sharma, Caves, Greene, & Fernando, 2018).

$$Qar=10\log_{10}(I_2/I_1)$$

Another ACD technique is times-series which is more sophisticated than pairwise ACD. As the name suggests time series is basically a series of data sets in time order, i.e., it's a sequence of samples taken successive and equally spaced in time. This technique is used for increased sensitivity to persistent changes such as new infrastructure or cleared land (Sharma, Caves, Greene, & Fernando, 2018). Like pairwise ACD, time-series ACD uses more than one SAR acquisitions, with the same geometry, to compute and identify the changes through time. The difference is that time series ACD uses more than two, in order to identify the dim changes such as vegetation growth, melting snow or the construction of new man-made structures, a minimal of 4 samples is needed for computing the variances (Sharma, Caves, Greene, & Fernando, 2018). In order to realize the dimension that this method can take, figure 26 represents a change map compiled from approximately 2.5 years of data showing the construction of a new interchange connecting routes A44n and A61 south of the mine of Bundesamt.

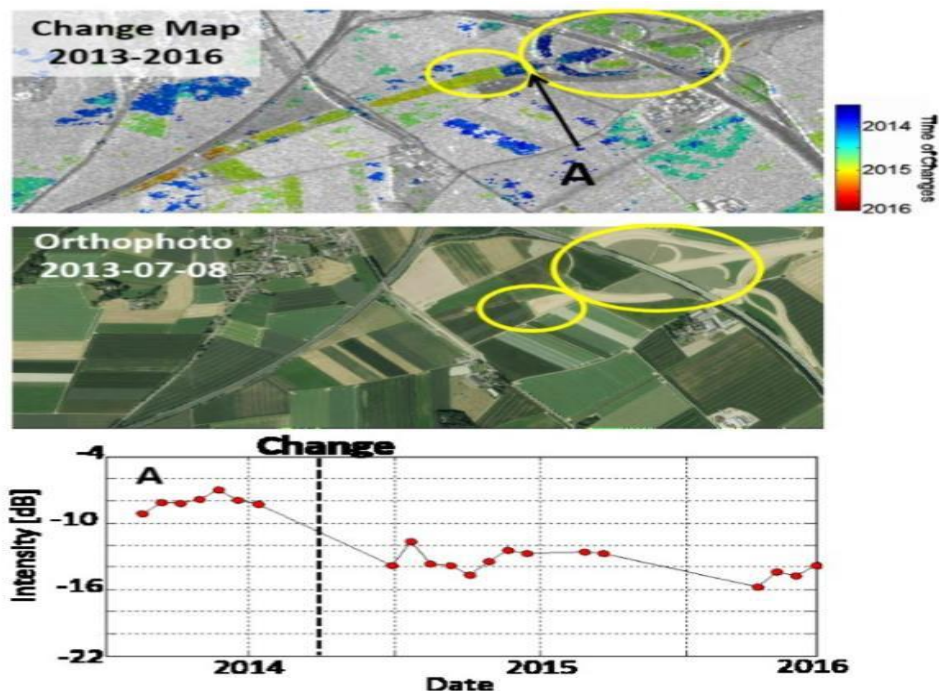


Figure 26 - Time Series applied to RADARSAT-2 XF data for infrastructure monitoring. TopImage:Radar change map; Middle Image: orthophoto from Bundesamt für Kartographie und Geodäsie; Bottom Image: SAR time series at location A.

CHAPTER 3

Techniques Evaluation And Selection

This chapter is divided into two sections: first, the structuring and creation of the Basis Guideline, based on the previous study; second, an analysis of the data that was selected to work will be made in order to choose a technique to implement on the chosen data type. The Basis Guideline will provide a choice process of a specific technique based on its characteristics such as advantages, disadvantages, scenario of application and type of data that is used. And it is through this guide that the technique to be used is chosen, accordingly with the outcomes of the pre-analysis of the chosen data. Note that regardless the techniques mentioned in chapter 2, it's important to keep in mind that there are more methods and variations, but its basic principles are based on the techniques that were briefly covered in chapter 2.

3.1 Basis Guideline

After the brief description of each technique, the major conditions to compare and evaluate each aspect, characteristic, vantages, disadvantages and other features of each respective method are gathered. Furthermore, the primal objective of these analyses is to determine the best technique for both the type of data that is going to be used and the scenario that is going to be analyzed.

After analyzing and studying each of the most used techniques, it is possible to highlight several aspects that characterize each one of them. For multi-look imaging, the major advantage over other conventional techniques is its ability to extract ships even when their images are embedded in noise and also estimate their velocities. CFAR techniques have variations that can be applied in different situations in order to achieve the most accurate results, depending on the target scenario, besides requiring low computational processing. Polarimetric techniques are applicable not only for ships detection but also for its characterization, as well as to detect other man-made structures. It can even perform oil spill detection and characterization but require heavier computational processing and it is mathematically more complex. Last but not

least, ACD techniques like pairwise ACD method has the most suitable applicability for ship detection as well as good results in harbor scenarios.

In Table 2 is created a basic guideline where it is summarized each one of the studied methods accordingly to its advantages, disadvantages, applicable scenario, i.e., area of interest and the type of data where the methods can be implemented with.

Type of Technique	Advantages	Disadvantages	Scenario	Type of Data
Multi-look	<ul style="list-style-type: none"> -Detection of static targets. - Target detection even if embedded in noise. 	<ul style="list-style-type: none"> - Low resolution results. - Medium computational requirements. 	<ul style="list-style-type: none"> - Far from Land. - Near Coast areas. 	<ul style="list-style-type: none"> - Complex data.
CFAR	<ul style="list-style-type: none"> - Good identification for stationary and moving targets. - Good response to noise interference. - High-resolution results. - Low computational requirements. 	<ul style="list-style-type: none"> -Unable to characterize the objects detected. - Unable to estimate the velocity of ships. 	<ul style="list-style-type: none"> - Far from land. - Near Coast areas. -Harbor scenarios. 	<ul style="list-style-type: none"> - Amplitude data.

Polarization	<ul style="list-style-type: none"> - Discriminates targets (buoys, ships, oil-spills, etc). - Characterization of targets. 	<ul style="list-style-type: none"> - Heavy computational weight. 	<ul style="list-style-type: none"> - Far from land. - Near Coast areas. 	<ul style="list-style-type: none"> - Complex, polarimetric data.
ACD	<ul style="list-style-type: none"> - High-resolution results. 	<ul style="list-style-type: none"> - Medium Computational requirements. - Needs a times series of SAR data of same geometry. 	<ul style="list-style-type: none"> - Harbor scenarios. 	<ul style="list-style-type: none"> Amplitude data.

Table 2 - Basis Guideline

With this information, remote sensing researchers, engineers, or even operational decision-makers will have a basic guide for selecting the best algorithm for the problem at hand. For example, if the available data is polarimetric type data (Complex data), it is obvious that the best choice is a polarimetric technique, but if it's amplitude SAR data images, CFAR techniques may be the suitable choice not because it presents significantly less computational weight but it also presents high-quality results in terms of visualization. According to the analysis of the area of interest, other techniques will come in handy. For example, if the purpose is to monitor movements in a harbor in a period of time, Pairwise ACD method presents good results with high quality, but if the goal is to estimate velocities, for example, multi-look imaging technique does the job. It's by following this line of thinking the users are able to choose the method that will provide better results on their tasks.

3.2 Technique Selection

The chosen data set to apply the presented basic guideline is from Sentinel-1. This data set was selected because it is freely available and of high-resolution. For processing Sentinel-1 data samples, the technique that is going to be used is CFAR. The reasoning for choosing CFAR is justified in the next sections. An analysis of the data regarding its type and characteristics is performed, and the scenarios of interest are defined. Through this analysis and taking into account factors such as available computing capacity, ease of implementation and the type of data obtained and the possibility to offer good results in all types of scenarios, it was chosen the CFAR methods once it seems to promise better results to the tasks on hands.

3.3 Data Analysis

Sentinel-1 constellation is composed by the Sentinel-1A, launched on 3 April 2014, Sentinel-1B, launched on 25 April 2016, and Sentinel-1C and 1D which are in development with launch dates to be determined. They are polar-orbiting satellites operating day and night performing C-band synthetic aperture radar imaging (ESA - European Space Agency, 2018), i.e., they operate at specific wavelengths which offer the ability to provide weather independent (like cloud cover or lack of illumination) images. These Satellites operate in four exclusive modes, Strip Map mode (SM), Interferometric Wide swath mode (IW), Extra-Wide Swath mode (EW) and Wave mode (WV), where its images have various resolutions, down to 5 meters, and can cover up to 400 kilometers. A set of wavelengths is denoted by Band, which have different beam modes that are defined by the swath width and spatial resolution. Sentinel-1 carries a single C-band synthetic aperture radar instrument (C-SAR instrument) operating at a central frequency of 5.405 GHz (5.5465763cm of wavelength). C-SAR instrument provides fast scanning in elevation and azimuth and it includes a right-looking active phased array antenna imaging (ESA - European Space Agency, 2018), i.e., a computer-controlled array of antennas which creates a beam of radio waves that can be electronically steered to point in different directions without moving the antennas (Balanis, Constantine A., 2015), as shown in figure 27 where A is the array of antenna elements, TX is the transmitter, C is the computer that controls

the phase shifter (ϕ) and θ is the antenna axis angle which is constantly changing accordingly to the change of the phase shifts.

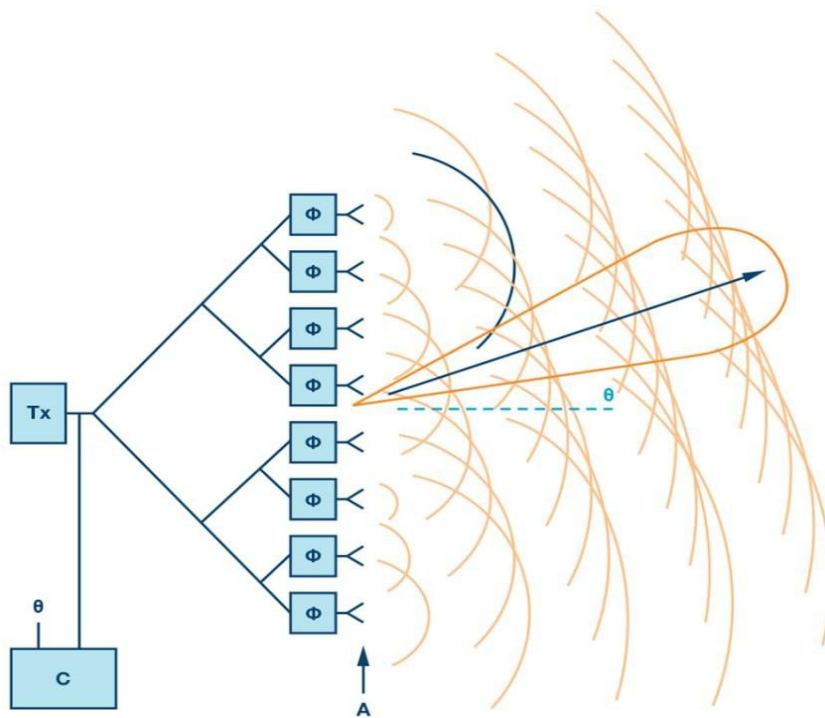


Figure 27 - Illustration of a phased array. Source: (Benson, 2019)

Figure 28 is a visual representation of the Sentinel-1 operating modes, where it's shown how the swath of each mode is acquired in order to provide de images of the covered area.

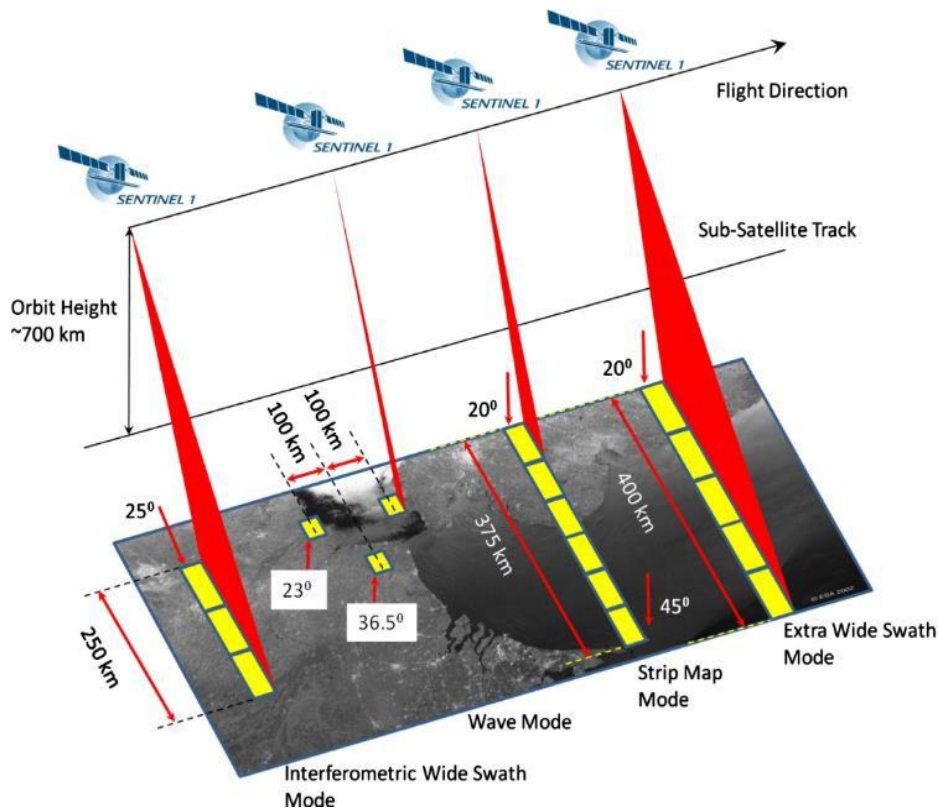


Figure 28 - Sentinel 1 operating modes.[ESA 2018]

Extra Wide Swath Mode (EW) is the one that has the biggest ground range cover (swath), approximately 400km, but with a lower pixel resolution, approximately 20 meters by 40 meters, then comes the Strip Map mode (SM) with a swath of 375km and with a pixel resolution of 5 meters by 5 meters. Interferometric Wide Swath (IW) mode works similarly to the EW but instead of having a total of five sub-swaths it has only three, providing a better pixel resolution (10 meters by 10 meters) but a smaller swath (250 km). Finally, the Wave mode (WV) which is composed of Strip Map segments of 20 km by 20 km, acquired alternately on two different incident angles (ESA - European Space Agency, 2018).

For each mode, with the exception of the wave mode, there are 3 types of core products, level-0, level-1, and level-2. Level-0 is the raw data, i.e., it's data that at first sight cannot be used, it needs to be decompressed and processed by a SAR processor in order to be usable. Level-1 products are the result of this decompression and processing of level-0 data. First, it's done a pre-processing of the raw data (level-0) and the internal calibration, then Doppler Centroid Estimation which results in range

and azimuth processing, finally, after this processing, final level-1 products are acquired. Figure 29 represents the workflow of this process.

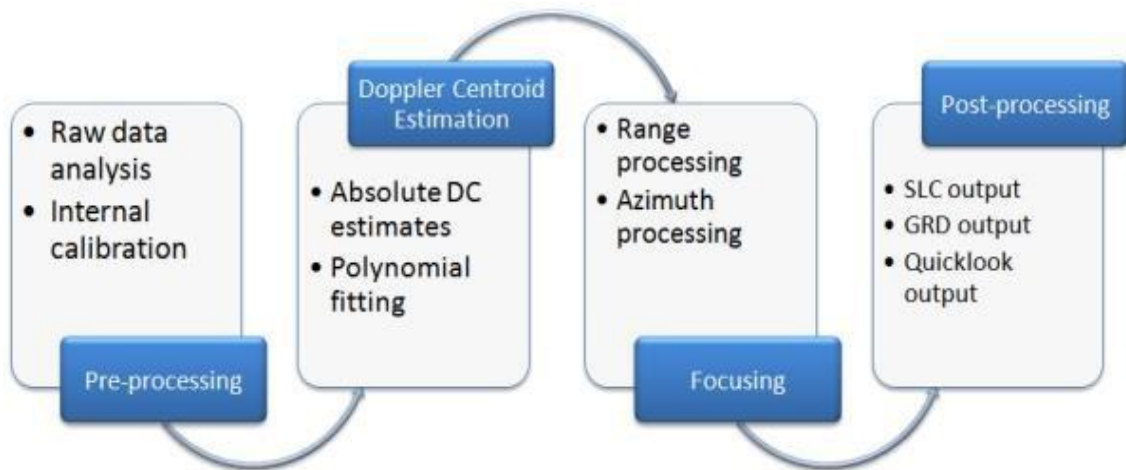


Figure 29 - Processing Flow

There are two types of level-1 products, Single Look Complex (SLC) and Ground Range Detected (GRD), where SLC products consist of focused SAR data georeferenced using orbit and attitude data from the satellite and provided in zero-Doppler slant-range geometry and preserves the phase information (ESA - European Space Agency, 2018) and GRD products consist of focused SAR data that has been detected, multi-looked and projected to ground range using an Earth ellipsoid model and phase information is lost (ESA - European Space Agency, 2018). GRD products can have Full, High or Medium resolutions (FR, HR, and MR) depending on the operating modes (MR and HR for IW and EW modes, MR for WV and MR, HR and FR for SM mode) (ESA - European Space Agency, 2018). Finally, level-2 products are more redirected to analyze wind velocity and direction which basically are derived geophysical parameters derived from Level-1 data.

Figure 30 gives an overview of all the sentinel1 core products and some of their characteristics.

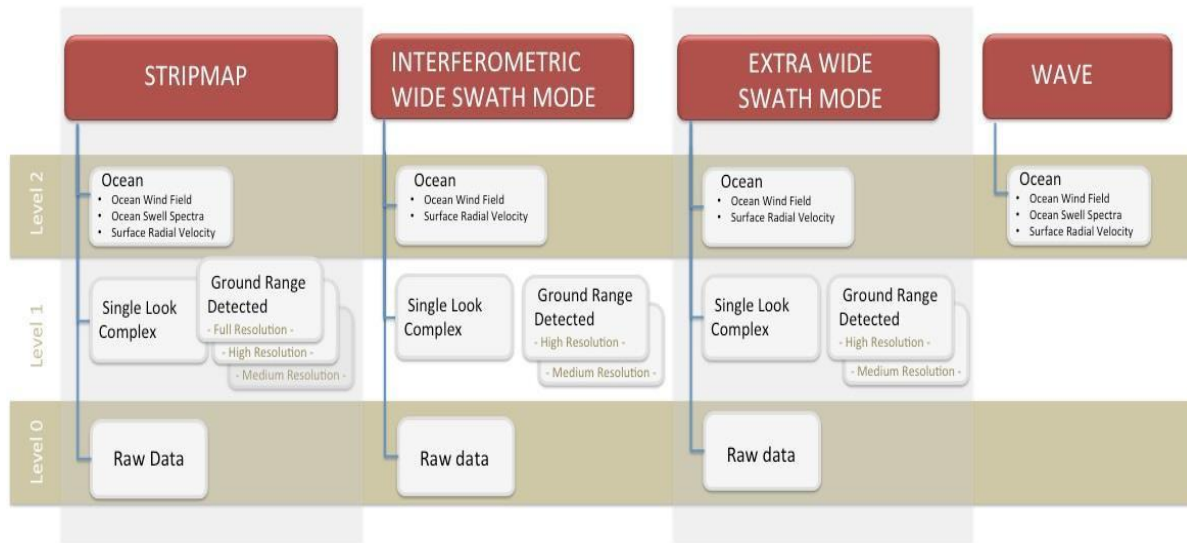


Figure 30 - Graphical Representation of Sentinel-1 Core Products.

Accordingly to this description and analysis of the types of products that Sentinel-1 can provide, the chosen products will be IW GRD products. Since Level-0 (Raw data) products aren't available to public use, we exclude that option. Then Level-2 products aim more to the wind analysis whereas to detection or land/sea analysis, so it is clear that working with level-2 products is not the most effective for ship detection applications. Finally, since GRD products provide FR and HR images and can discard phase information to do so, the computational requirements and the processing speed will be lower whereas using SLC products. Furthermore, IW mode products will be used because it provides a reasonable spatial resolution (20x22 m) and pixel spacing (10x10 m) and also because in IW GRD products the three beams (IW1, IW2, IW3) form a single image that is "continuous" in comparison to IW SLC products as shown in figure 31.

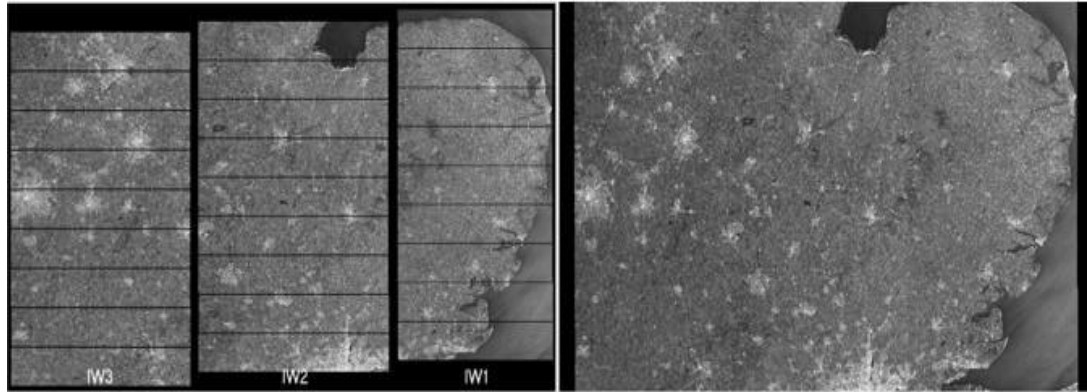


Figure 31 - IW products. Left side is IW SLC bursts and sub swaths. Right side is the IW GRD product

It also important to mention that IW GRD products can present VV or HH polarization. Since HH polarization permits the best ship-sea contrast, whereas VV polarization provides more information on sea surface conditions, the images with HH polarization were chosen to test the implement algorithm.

3.4 Scenario of application

The purpose of this work is to provide a practical and simple tool to improve the performance of the Portuguese Navy in its tasks or missions. Portuguese Navy is responsible for numerous activities and missions, like detection and monitoring for illegal fishing activities, drug trafficking, human trafficking, control of maritime traffic, search and rescue operations and military operations (Marinha, 2019); basically Portuguese Navy is responsible to promote navigation safety and sea monitoring for any suspicious activities. Portugal Navy Exclusive Economic Zone (EEZ) is the third-largest zone in the European Union (EU) and eleventh largest in the world with a total of 1,727,408 KM² where 327,667 KM² are continental waters, 953,633 KM² are Azores waters and 446,108 KM² are Madeira waters. Furthermore, there is a proposal to increase its EEZ to double, approximately 3,877,408 KM². Figure 32 shows Portugal EEZ and the proposed platform extension(BMar, s.d.).

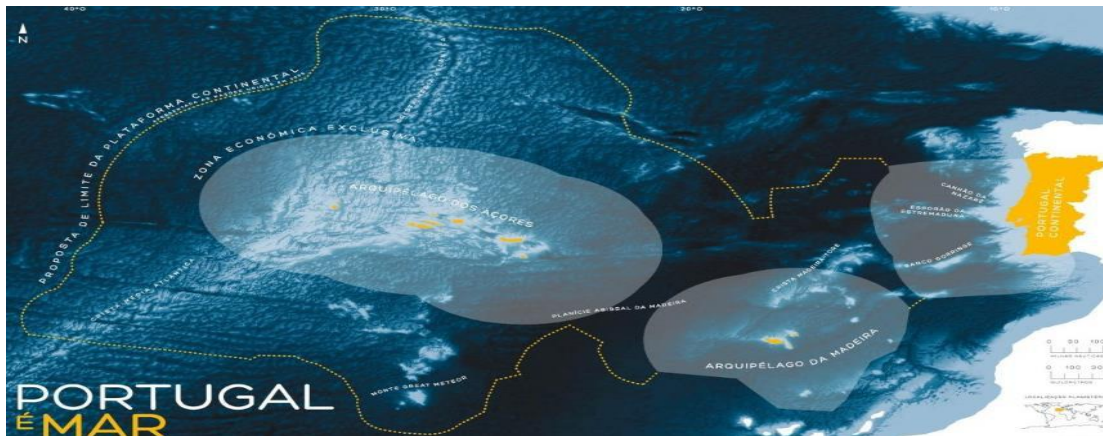


Figure 32 - Portugal EEZ and the proposed platform extension (*Noctula - Consultores em ambiente, 2018*).

From the size of the EEZ, it is clear that, possibly, several commercial routes and any other type of maritime traffic crosses the Portuguese maritime area, which makes a challenging task to permanently monitor them. Figure 33 gives an overview of several commercial routes around the world where it is possible to see its density on Portuguese waters.



Figure 33 - Comercial Routes around the World (*The spatial organization of transportation and mobility, 2018*).

In summary, the scenario of application of interest, accordingly with the basic guideline created, is far from land zones and near coast land zones, because it is where most of the activities take place.

CHAPTER 4

THE ALGORITHMS

4.1 Introduction

This chapter provides a detailed description of the implemented algorithms in terms of methodology and techniques. Given the type of the data and the scenarios of interest explained in Chapter 3, the CFAR technique was chosen. Furthermore, Annex 3 presents a guide on how to obtain and extract the Sentinel-1 data required for this study.

In order to work with the Sentinel-1 GRD data, the following functions were implemented and figure 34 explains the algorithm structure:

- 1.*Read Files*: reads the selected SAR image from the Sentinel-1 packagedata;
- 2.*Dynamic Division*: performs multiple divisions of the original Sentinel1 SAR image, i.e., divides the SAR image into sub-images with smaller size;
- 3.*GAUSSIAN CFAR*: processes the image through a CFAR method using a gaussian distribution;
- 4.*K-MEANS GAUSSIAN CFAR*: processes the image through a K-means methodology and then implements the CFAR technique.
- 5.*Contact Type*: analyses the detections made by the previous algorithms and characterize them in terms of size.

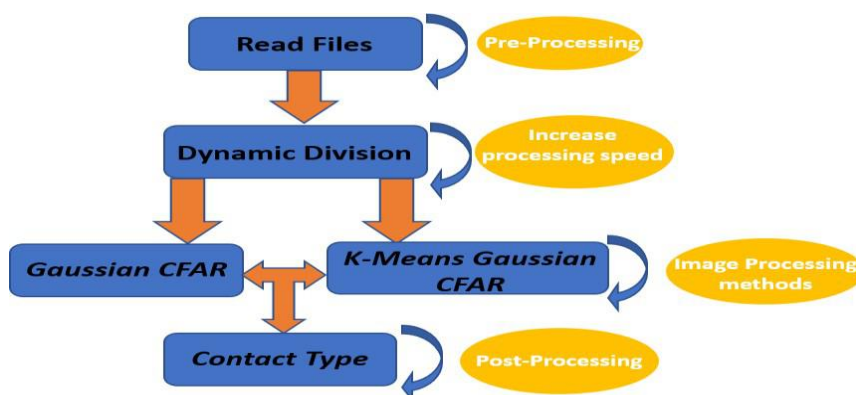


Figure 34 - Algorithm's Interaction structure.

Sentinel packages consist of a set of files where many of them have the information needed to apply the calibration to the image obtained as well as the measurements for the determined polarization. Besides all that files, Sentinel-1 also offers a quick-look which is a colored image from the area but with a lower resolution.

Before using the SAR image present in any downloaded Sentinel-1 package, a program called SNAP (ESA, 2019) was used in order to perform the conversion of the image into the preferable MATLAB type, uint8², and also to speed up the image processing and make it more efficient, because the size of the SAR images that we are working on have sizes between 1.5Gb and 2Gb. These images have high-detailed and high-resolution features and its processing requires some computational power. SNAP provides the possibility to extract the SAR image without loss of the geo-reference and with the internal calibration implemented which is related to the internal Sentinel radar configurations and orbit features and settings. Furthermore, it converts the SAR images from uint16³ to uint8 which is a great boost to increase the speed of the image processing, because it reduces the memory requirements needed and no information is lost. Figure 35, is a print of the SNAP program where all operations and configurations that were done are highlighted: the radiometric calibration in blue and the extraction of the “GeoTIFF” in red.

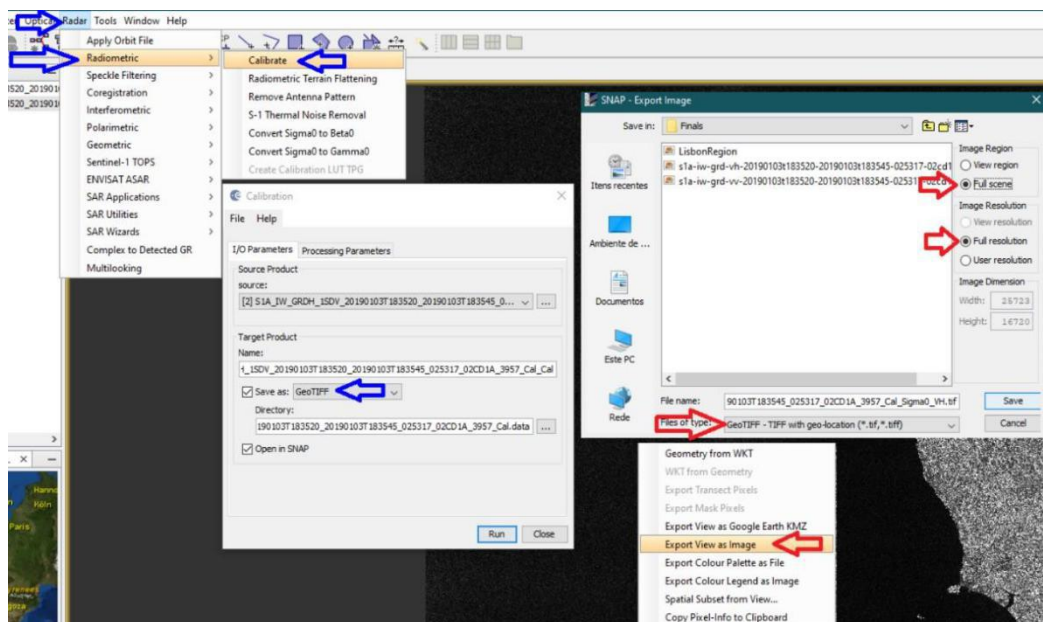


Figure 35 - SNAP Operations and Configurations.

² Represents an unassigned integer number stored with 8bits, meaning that value has a range between 0 and 255.

³ Represents an unassigned integer number stored with 16bits, meaning that value has a range between 0 and 65525.

Annex 1 presents all the code developed. It is divided by sections as mentioned above with the exception of the Contact type that is implemented within the functions 3. and 4. The following sub-chapters will describe and explain the full algorithm, i.e., the methodology and techniques, as well as the mathematical formulas that were used and implemented.

4.2 Read Data processing function

After extracting the final SAR image from the Sentinel-1 package using the SNAP program, the Matlab processing begins. Initially, the SAR image is read with an adaption of the function called “*GEOTIFF_READ*”, a version made by Yushin Ahn, Glacier Dynamics Laboratory, Byrd Polar Research Center, Ohio State University and it is also read with a Matlab function called “*imread*”. The first function is used to attribute to each pixel a set of coordinates, latitude, and longitude. The geographic information is stored in a referential system where in y is stored the longitude of each pixel and in x is stored the latitude of each pixel. In z is stored the backscattered value of each pixel. After storing the geographic reference of each pixel, a mouse track function is applied to the image which allows the user to know the coordinates while navigating through the image with the mouse cursor.

The second function reads the image as a matrix, after being georeferenced, in order to reduce it into a matrix with only one band instead of having four bands. By doing this we increase the speed of the processing and no information is lost because Sentinel SAR images are in grayscale, this means that all bands of the CMYK (Cyan, Magenta, Yellow, Black) color band system have the same value, i.e., each band of the four bands matrix is equal. After this, the orientation of the image from the Sentinel-1 SAR geometry is shifted to the user normal orientation (north up). Figure 36 shows the SAR geometry visualization that was acquired and the rotation applied. In

figure 37, the output obtained by applying the code in Annex 1, section “Read Files Code Set” is presented, where in the red box is represented the coordinates that change accordingly to the position of the cursor in the image.

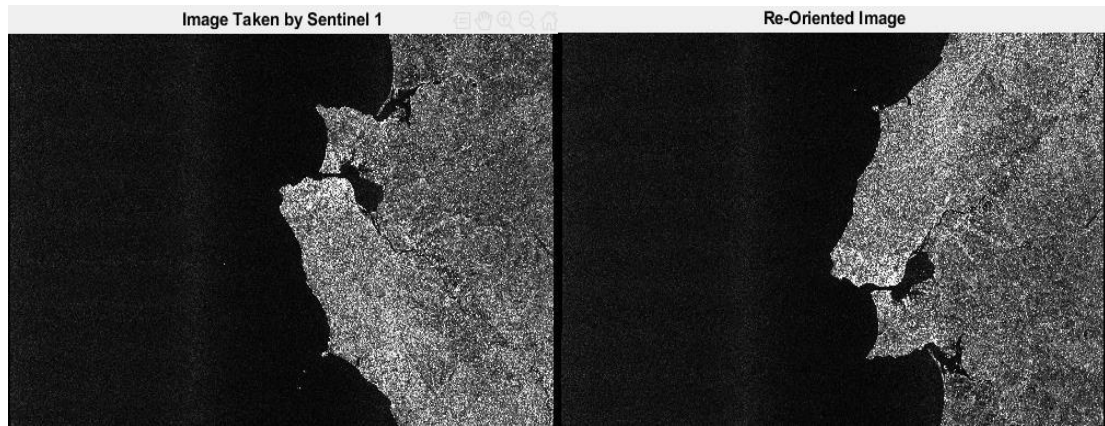


Figure 36 - Sentinel SAR image visualization, acquired in a descending pass.

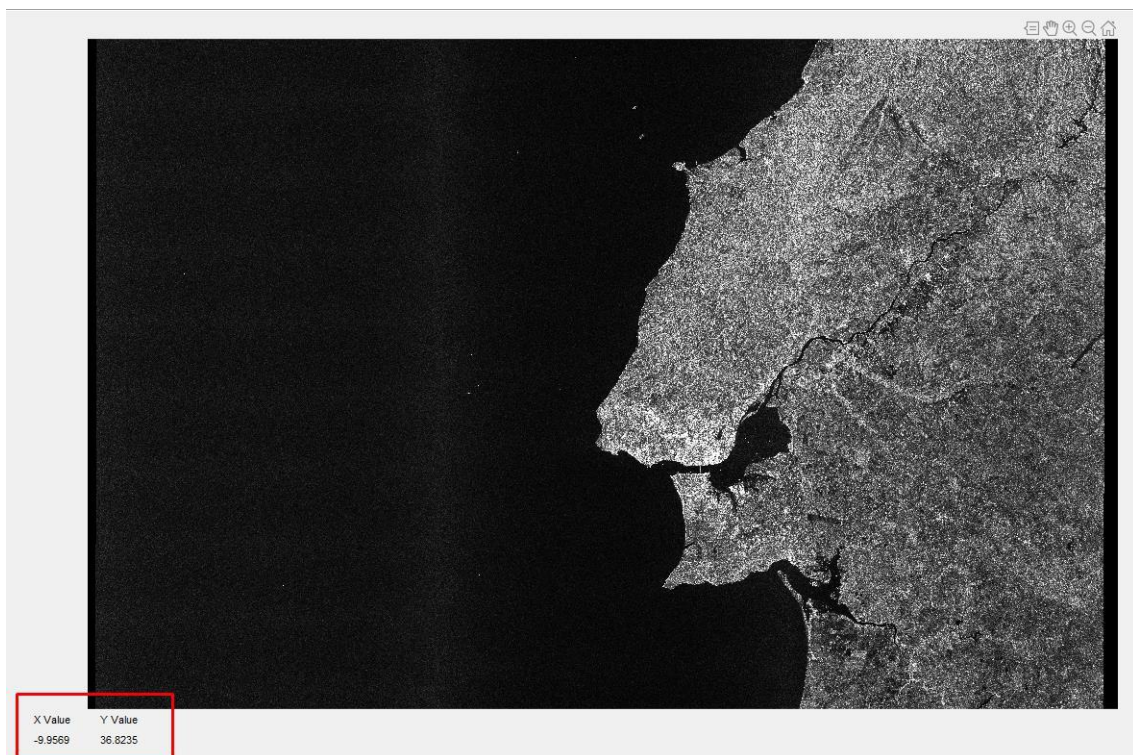


Figure 37 - Sentinel-1 SAR image read from Matlab.

4.3 The dynamic Division processing function

After reading the image and georeferencing each pixel, a division by blocks to the original image is implemented. This is done because the original image has

extremely big dimensions to be processed in full by the following algorithms that were implemented to perform ship detection and also to allow the users to choose the zones of interest to analysis. The time to process the entire image for ship detection using a cutting-edge laptop with 64Gb of RAM, sixth-generation intel corei7 with a 3.2GHz clock speed and 16Gb of graphic memory⁴ was 10092seconds which correspond to approximately 2 hours and 48 minutes. Giving the time requirements it seems wise to process the image by blocks or segments, so the division that was applied was based on the image dimensions and the resolution of each pixel.

As mentioned in chapter 3 the chosen SAR images have a ground range coverage of approximately 250 Km and 10x10 meters of pixel resolution. The corresponding *Matlab* matrixes for the full SAR images of the Sentinel-1 packages have dimensions of 16720x25723. This means that each image covers an area of approximately 43008,86 Km^2 which is almost half of Portugal Continental area (92212 Km^2). Thus, taking into account the image processing time and its dimensions, the presented code in Annex1 divides the full image into segments with dimensions of 1081(plus the clutter zone size)x1921(plus the clutter zone size) pixels which means that the algorithm processes approximately 207,66 Km^2 at a time and the time process of each one of these segments are approximately 37 seconds. This image size is also used because it's the standard size for high definition images on a common laptop. Note that the given time references are only meant to provide a palpable notion of the needed processing time because if the user runs the algorithms in a different laptop the processing time will vary. Furthermore, the user can change the dimensions of each segment by changing the values of two initialization variables shown in figure 38.

```

17      %%Size for Columns%%
18      xsize = 1920;
19
20      %%Size for Rows%%
21      ysize = 1080;

```

Figure 38 - Segment Dimensions.

The user can use the following equation to choose the Segment dimensions accordingly to the area size

$$Segment_{Area}(Km^2) = (xsize \times 0,1) \times (ysize \times 0.1)$$

where $xsize$ is the number of pixels for the columns (horizontal direction) and $ysize$ is the number of pixels for the rows (vertical direction).

The clutter zone size is a variable that will be explained in the next section. In the division process this variable is only used to prevent parts of the image from not being processed, i.e., the dimension of the segment will have the chosen $xsize$ and $Ysize$ dimensions plus the clutter zone size but the area that will be processed and analyzed will only be the area covered by the $xsize$ and $ysize$ values. With these operations, all the original image can be processed and analyzed with the exception of its real borders and not the borders of each segment created, because each segment includes part of the neighbor's segments.

The final product of the implementation of the dynamic division algorithm is a vector where in each position is stored a segment of the original image and plot of all the created segments, shown in figure 39, for the user to visualize them in order to help choosing what segment the user intends to analyze with the Gaussian CFAR and/or the K-means with Gaussian CFAR algorithms.

4.4 Gaussian CFAR function

After the image is fully georeferenced and divided into segments with the pretended size, ship detection is the next step. For this, it was applied a CFAR technique for the reasons discussed in chapter 3. Before explaining the code methodology used, it's essential to understand how this technique performs the image analysis. As mentioned in Chapter 2 section 2.3.2, CFAR techniques compute a threshold that allows to determine if there is a possible target detection in the area under analysis. To increase the efficiency of this technique the threshold can't be always the same for the entire image, it has to be dynamic, i.e., the threshold must vary accordingly to the zone of the image. This means that the threshold is dependent on the surrounding area of the pixel under analysis. So, in practical terms, what a CFAR technique does is to search for pixels that present a higher value than the threshold established for its surrounding area. If the pixel presents a higher value than the established threshold, it means that it is a possible target detection, otherwise, it's not a possible target detection.

Depending on the image resolution, more specifically the pixel resolution, and the type of targets intended to detect, it is needed to establish an area around the pixel under evaluation that does not contribute for the computation of the adaptive threshold, the guard zone, and then establish an area bigger than the guard zone but not too big, so the analyses of the image remains local, this area is commonly called clutter zone or background window. It's the pixels inside this zone that will contribute to computing the threshold of the surrounding area of the pixel under analysis.

To give an example, if the purpose of the algorithm is to detect ships, the guard zone size will be similar to the size of the biggest ship and the clutter zone size will be significant larger than the guard zone in order to establish a good threshold but not too big so the analysis in the image remains local. Figure 40 illustrates the “windows” that are created around the pixel under analysis, as the pixel under analysis changes the “windows” move accordingly.

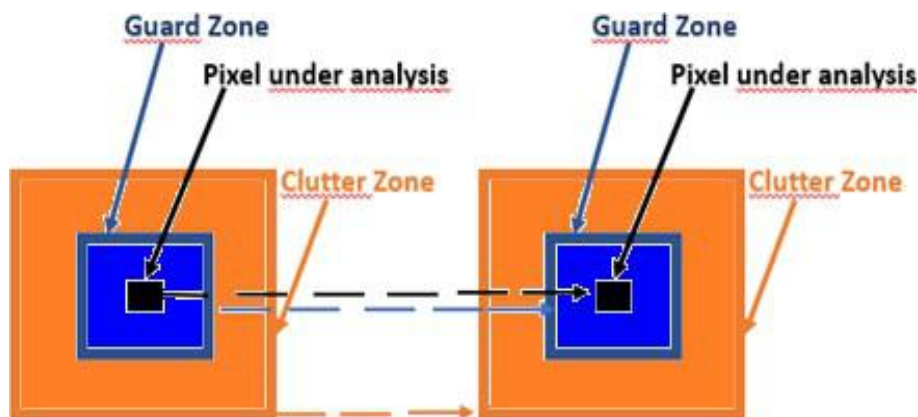


Figure 39 - CFAR Window formation process.

Once understanding the CFAR analysis process, it is necessary to explain how the threshold computation is done. This process is accomplished with the use of probability density functions (pdf) like the gaussian distribution, also called normal distribution, the k-means distribution, the alpha-stable distribution, t student distribution, Rayleigh distribution, among many others.

For the ship detection process, the gaussian distribution was used as it usually delivers reliable results when dealing with a large number of samples. This is

the case as the working data is a set of high definition SAR images and the algorithm will be applied to a large number of pixels.

Like any other pdf, gaussian distribution is a statistical method, a function that specifies the probability of a random variable falling within a particular range of values, as opposed to taking on any other value. A pdf is commonly represented by the following equation:

$$F_X(x) = P[a \leq X \leq b] = \int_a^b f(x) dx$$

where μ is the expected value, known as the mean value which is calculated by the following formula:

$$\mu = \frac{\sum_{i=0}^i x_i}{n} = \frac{\text{sum of data}}{\text{number of data points}}$$

and sigma is the standard deviation which is calculated by the following equation:

$$\sigma = \sqrt{\frac{1}{N} \sum_{i=1}^N (x_i - \mu)^2}$$

Graphically speaking, figure 41 translates the result of a standard Gaussian distribution, where approximately 68%, 95% and 99.7% of the values are within the intervals $[\mu - \sigma; \mu + \sigma]$, $[\mu - 2\sigma; \mu + 2\sigma]$ and $[\mu - 3\sigma; \mu + 3\sigma]$, respectively.

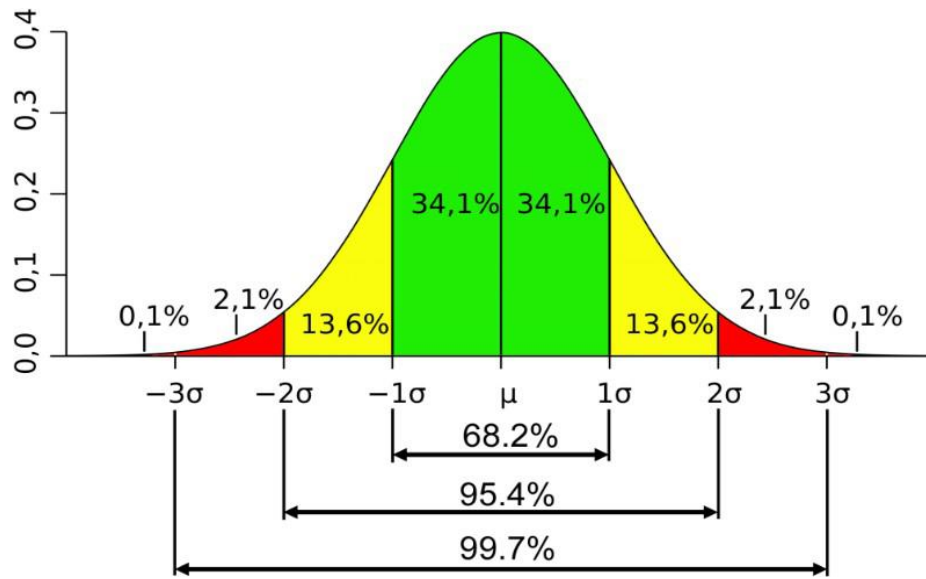


Figure 40 - Standard diagram for Gaussian distribution.

Giving all this, the CFAR numerical method solution to determine if there is a possible target detection or not, using the Gaussian distribution, is obtained by the following equation:

$$\underline{x_t} > \underline{\mu_b} + \underline{\alpha\sigma_b}$$

where if X_t , the pixel amplitude value under analysis, is bigger than the sum of μ_b , the background mean, i.e., the mean of the clutter zone values, and σ_b , the background standard deviation, also from the clutter zone values multiplied by alpha, an empirical value that will be evaluated in the next chapter and which value will contribute to more accurate detections.

Regarding the code implementation for this process which is in the Annex 1 section 3, first it's performed the reading of the segment that is intended to be analyzed and set the initial variable values:

Possible_detection: Matrix that will store every pixel position that might be a possible target detection;

Comparison_Matrix: Matrix that will store the difference between the pixels values that are considered to be possible target detections and the value that defines whether the pixel is considered as possible target detection or not;

GuardZone: Matrix of the guard zone window around the specific pixel;

ClutterZone: Matrix of the background window around the specific pixel.

The guard zone matrix size was defined accordingly to the average dimensions of the biggest ships that currently exist, like the OOCL Hong Kong container ship with a length of 399 meters and a breadth of 59 meters, the COSCO Shipping Universe container ship with a length 400 meters and a breadth of 58 meters, the Allure of the Seas cruise ship with a length of 362 meters and a breadth of 65 meters, among many others. Giving this *a priori* information and the pixel resolution the guard zone and the clutter zone size were set to 20 and 40, respectively, this means that the windows will have 18x18 and 36x36 pixels dimension, respectively. These dimensions were chosen because the area of the biggest ships is around 26000 KM² and since each pixel is 10x10 meters a box with 18x18 pixels with cover an area of 32400 KM² which is slightly bigger than the area of the biggest ships and the clutter zone dimensions are the double of the guard zone dimensions to provide enough samples to compute a good threshold and still maintain the image analysis to be local.

After defining the guard zone and clutter zone size, it necessary to establish the initial and the end pixel so the image boundaries are not exceeded. Giving the window formation in figure 39 it's easy to understand that starting in the first pixel of the image segment will not be possible to form the windows correctly so, to avoid adding more exceptions and conditions that will slow the algorithm, we set the algorithm to start and end the image process as shown in figure 41.

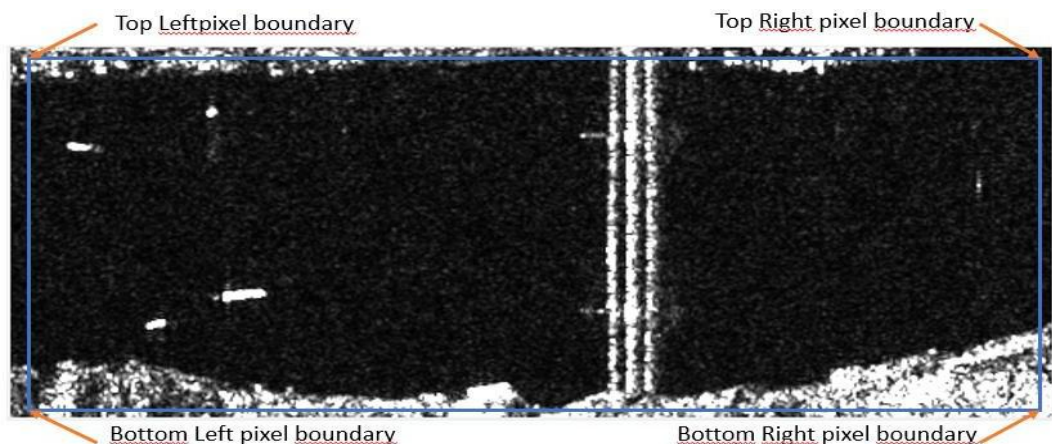


Figure 41 - Processing Image delimitation.

This delimitation is done accordingly to the size of the biggest window, the clutter zone. Figure 42 shows the code lines that do this delimitation process, and in order to move the window formation while changing the pixel under analysis, Matlab “FOR” cycles mentioned in the Annex 1 section 3, are used.

```
Begin_rows = (ClutterZoneSize/2) + 1;
End_rows = Test_rows - (ClutterZoneSize/2);
Begin_collumns = (ClutterZoneSize/2) + 1;
End_collumns = Test_collumns - (ClutterZoneSize/2);
```

Figure 42 - Code lines to establish the pixels for each image corner.

In order to use equation 13 to determine the pixels that might be possible target detection, we calculate the mean and the standard deviation for each pixel surrounding area. The steps to calculate the mean and the standard deviation of the surrounding area, respectively.

The result of the implementation of this function is an image that outputs the target detections as shown in figure 43, where each one of them is numbered and boxed to give a better visualization of the target position.

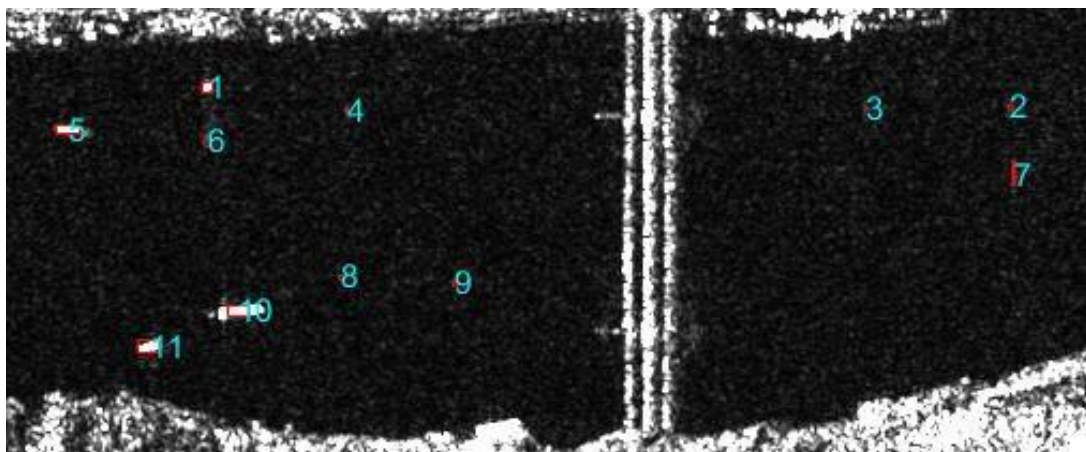


Figure 43 - Example of the output resulting from the Gaussian CFAR algorithm implementation, alpha= 6.

4.5 K-means with Gaussian CFAR function

The next method to analyze the SAR images is by applying K-means clustering to the image before processing it by the implemented Gaussian CFAR algorithm. The method was chosen because it's relatively simple to implement, it's faster to compute

when the sample has a large number of values, it guarantees convergence of data and easily adapts to any kind of data given. In our case we use k-means clustering to divide the image into 3 clusters, i.e., the values of every pixel will be converted into 1, 2, or 3. The choice to only divide the images into 3 clusters is simple. In theory, the image should be divided into 2 clusters because it is intended to distinguish land from sea, sea from ships or land from ships. Since ships present high backscatter values similar to land (white color in a grayscale image) and sea presents low backscatter values (black color in a grayscale image) dividing the image into 2 clusters would serve the purpose but in practice this isn't efficient because there is noise in the image, i.e., there are a vast number of pixels that present a backscatter value in the middle zone. This is due to for example the sea state or the ships draft, so the third cluster is added in order to visualize this distinction. The resulting image will be then divided in 3 levels of grayscale: pixels with high backscattering value will appear as white, pixels with medium backscattering value as grey, and pixels with Low backscattering value as black. In simple terms, k-means algorithm can be summarized as follows:

STEP1: Cluster the data samples into the k groups where k is defined a priori by the users;

STEP2: Then the algorithm will choose randomly k data points to be the initial cluster centers, also called centroids;

STEP3: After setting the initial centroids, it will assign the remaining data points to the nearest centroid accordingly to the Euclidean distance function;

STEP4: Finally, the algorithm will calculate the mean in each k groups and the result will be the new centroid of each k groups;

STEP5: The algorithm will repeat the third and fourth step until there's a convergence of the data, i.e., when the new centroids are equal to the previous ones, or extremely similar.

Mathematically, after randomly choosing the k centroids, the algorithm will assign each pixel amplitude value, X_i , to the nearest cluster, C_k , accordingly to the following equation:

$\text{argmin}(X_i, C_k)$

where D is the distance function which in this case is used the Euclidean distance that can be obtained by the following equation:

$$D(x, C_k) = \sqrt{\sum_{i=1}^K (x_i - C_k)^2}, \quad K = 1, 2, 3$$

Then the algorithm will calculate the mean of each cluster and reassign its centroid to its mean and repeat those steps until there's no significant difference between the mean of the cluster and its centroid value, i.e., when both have the same value or very similar one.

Figure 44 shows the resulting image after applying this clustering. Visual and practically speaking, this technique removes the “noise” of the image making it more “digitalized”.

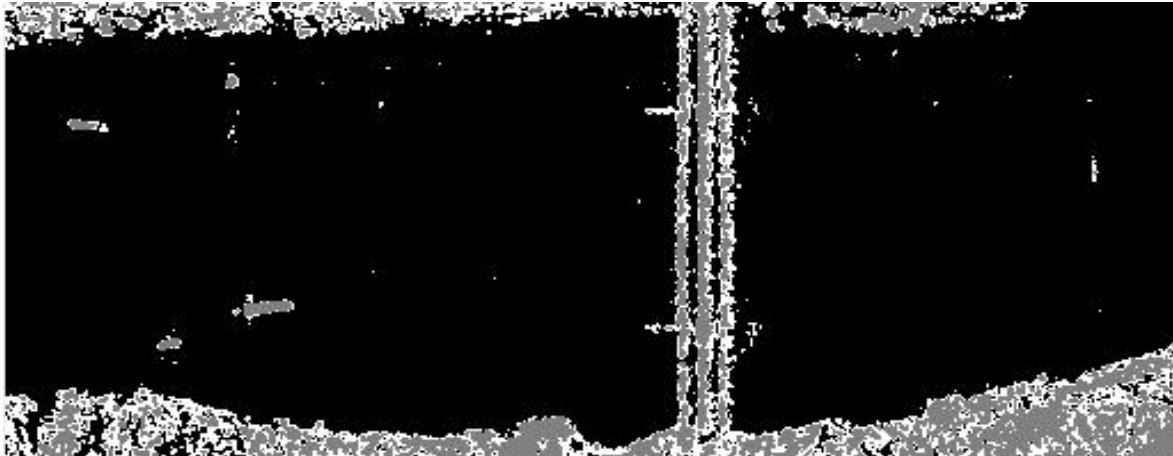


Figure 44 - Clustered Image.

After clustering the image segments, the Gaussian CFAR algorithm is applied, where the result is shown in figure 45. The code for this algorithm is listed in Annex 1 section 4.

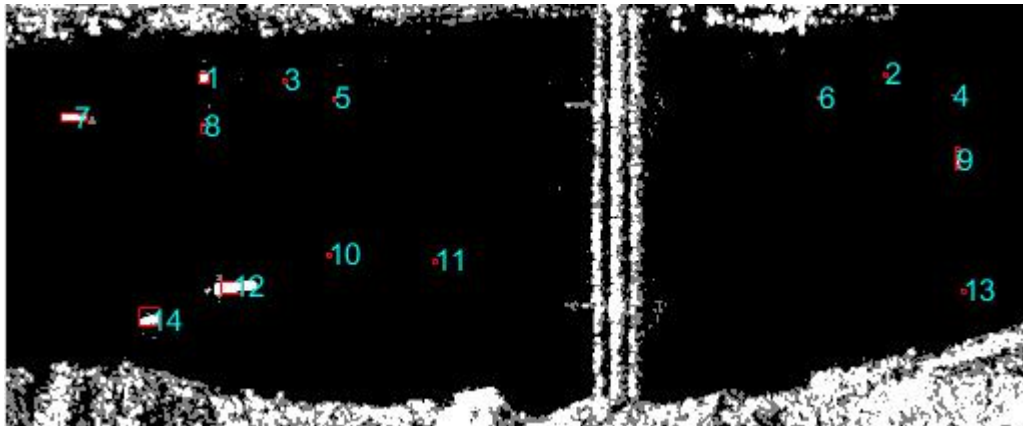


Figure 45 – K-means with Gaussian CFAR algorithm output.

4.6 Contact Type and Results

After the image processing by the previously explained algorithms, a simple criterion to classify the detections into Small ship, Medium ship, Big ship, and Giant Ship is created. The parameters that were to characterize the ship type were the number of pixels of each detection and the pixel resolution itself. The criterion is as follows:

Small Ships: Ships up to 80 meters in length;

Medium Ship: Ships between 80 and 140 meters in length;

Big Ship: Ships between 140 and 260 meters in length;

Giant Ship: Ships over 260 meters in length;

CHAPTER 5

Results



Figure 46-Original image



Figure 47-Median smoothing image



Figure 48-Thresholded image

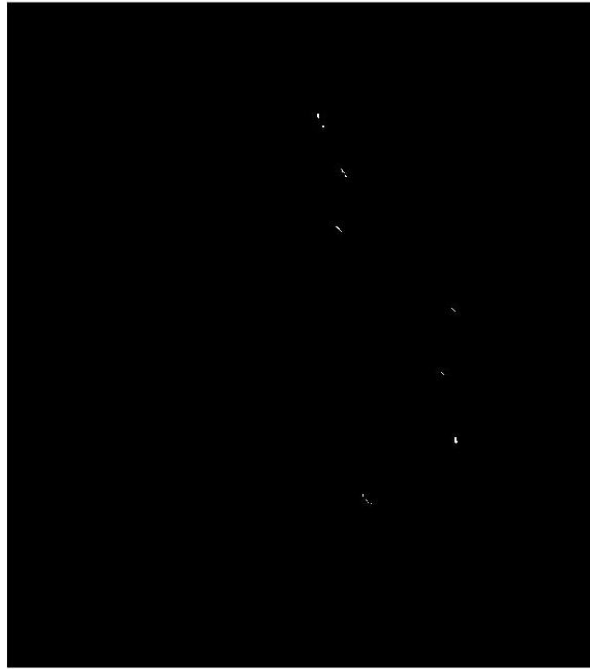


Figure 49 Morphological operated image

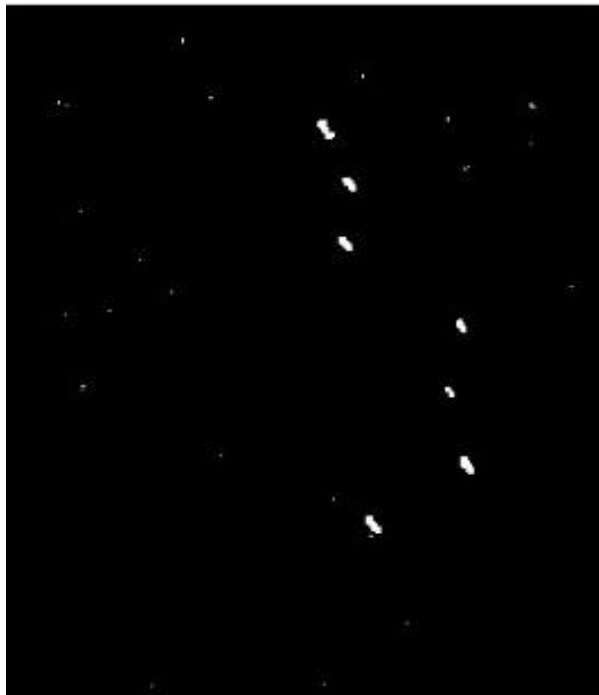


Figure 50 Output image

Chapter 6

Conclusions

In this report, we present a ship detection scheme ,CFAR PreScreening for spaceborne SAR imagery. It is able to process a wide range of spaceborne SAR data. The aim of this scheme is to solve the practical problems in ship detection. We have reviewed the general flow of ship detection in spaceborne SAR imagery and its problems. Accordingly, the works are completed in this report as follows.

The first one is an adaptive ship candidate detection method. It has two advantages mainly. The first concerns that the method is able to process several kinds of SAR images collected by different sensors. The second is related to that the method is able to detect potential ship candidates in a fast, efficient and robust way. Both make it a practical method for ship candidate detection in spaceborne SAR imagery.

The development of ship detection method can effectively detect ships despite the reduced image resolution of SAR image.

References

1. Air and Space Power Journal. (2019).
2. Alberto Moreira - German Aerospace Center (DLR). (2016). Synthetic Aperture Radar (SAR): Principles and Applications.
3. Balanis, Constantine A. (2015). Antenna Theory: Analysis and Design, 4th Ed. John Willey & Sons.
4. Benson, K. (2019). Phased Array Beamforming ICs Simplify Antenna Design.
5. BMar. (2018). *Maritime Zones under Sovereignty and or Portuguese Jurisdiction*. Retrieved from <https://www.dgrm.mm.gov.pt/am-ec-zonas-maritimas-sob-jurisdicao-ou-soberania-nacional>
6. Brown, W., & Porcello, L. (1969). An introduction to synthetic-aperture radar. *IEEE Spectrum*, 6 (9), 52-62.
7. Brown, E., & Fingas, M. (2013). Synthetic aperture radar. *IEEE transactions on Aerospace and electronic Systems*, AES-3 (2), 217-229.
8. Chan, Y., & Koo, V. (2008). An introduction to synthetic aperture radar (SAR).
9. *Progress in electromagnetics Research B*, 2, 27-60.
10. Cochenec, Y. (2019). Air & Cosmos.
11. E O College - Universitat Jena. (2017). Echoes in space. Introduction to radar remotesensing. Retrieved from <http://eo-college.org/course/echoes-in-space>
12. EMSA. (2018). *Copernicus maritime surveillance product catalogue*. Retrieved 2018, from www.emsa.europa.eu/cbs-menu/itams.html?cid=122&id=3025
13. ESA -Earth Online.(2018). *Radar Course 2*. Retrieved from <https://earth.esa.int/web/guest/missions/esa-operational-eo-missions/ers/instruments/sar/applications/radar-courses/course-2>

- 14.ESA- Earth Online.(2018). *Radar Course3*.Retrieved from <https://earth.esa.int/web/guest/missions/esa-operational-eo-missions/ers/instruments/sar/applications/radar-courses/course-3>
- 15.ESA-European Space Agency. (2018). *Sentinel Online*. Retrieved from <https://sentinel.esa.int/web/sentinel/missions/sentinel-1>
- 16.ESA. (2018). Interferometry.
- 17.ESA. (2019). *STEP - Science Toolbox Exploitation Platform*. Retrieved from <https://step.esa.int/main/download/snap-download/>
- 18.ESA Copernicus. (2019).*Copernicus observing the earth*. Retrieved from https://www.esa.int/Our_Activities/Observing_the_Earth/Copernicus/Overview4
- 19.ESA EOCollege. (2019). Echoes in Space Introduction to radar remote sensing.
- 20.European Space Agency. (2014). *Sentinel-1: Radar mission*. Retrieved from <https://sentinel.esa.int/web/sentinel/missions/sentinel-1>
- 21.F. Quina, J. P. (2019). A Look on Ships Detection techniques using SAR Images .
- 22.Goulão, S. (2018). RADARES DE ABERTURA SINTÉTICA (SAR): Os fundamentos e potencialidades de uso na Marinha Portuguesa.
- 23.Guissard, A. (1994). Mueller and Kennaugh matrices in radar polarimetry. Hecht, E. (2002). *Optics(4th ed.)*. United States of America: Addison Wesley.

APPENDIX

Method1

Main Function-

```
function ship_Detect(x, paf, r1, r2, A1, A2 )  
tic  
imageSmoothing(x);  
gaussianFit(x);  
CFAR(x,paf, r1, r2, A1, A2);  
toc  
End
```

Image smoothing-

```
function [x,y,m,s,l,w,test]=imageSmoothing(x)  
img=imread(x);  
h=ones(21,21);  
[l,w] = size(imread(x));  
test=conv2(img,h/441,'same');  
test = test/max(test(:));  
imtool(test,[]);  
imtool(x);  
figure(1);  
smooth=mat2gray(test);  
imshow(test,[]);  
imwrite(test,'boat3_VV_smoothing.tif');  
[y,x]=imhist(test);
```

```

gt=imhist(test);
m=mean2(test);%u
s=std2(test);%sigma
disp(m);
disp(s);
End

```

Guassian Filter-

```

function gaussianFit(in)
[x,y,m,s,l,w,test]=imageSmoothing(in);
y = y/(l*w);
plot(x,y);
xlim([0,0.1]);
fun=fitype('A*exp(-((x-u)/sigma)^2/2)');
options=fitoptions(fun);
options.StartPoint=[max(y) s m];
q=fit(x,y,fun,options);
disp(q);
i = 1;
county = 0;
countx = 0;
while(i < 256)
    if(y(i) < q.A)
        county = county + y(i);
        countx = countx + (m - x(i))^2*y(i);
        i = i + 1;
    end
end

```

```

else
    county = county;
    countx = countx;
    break;
end;
end;
B = sqrt(countx/county);
co=[q.A,q.u,q.sigma,B];
save('coefficient.mat','co');
End

```

Cfar-

```

function CFAR(in, paf, r1, r2, A1, A2)
tic
load('coefficient.mat');
T = norminv(1-paf, co(2), co(4));
disp(T);
[~,~,~,~,l,w,test]=imageSmoothing(in);
new = ones(l,w);
for i = 1:l
    for j = 1:w
        if(test(i,j) > T)
            new(i,j) = 1;
        else
            new(i,j) = 0;
        end;
    end;
end;

```

```

    end;
end;
imtool(new,[]);
[L,num] = bwlabel(new,8);
p = regionprops(L, 'Area', 'MajorAxisLength',
'MinorAxisLength');
s = cat(1, p.Area);
a = cat(1,p.MajorAxisLength);
b = cat(1,p.MinorAxisLength);
for i = 1:size(s)
    if(s(i) < A1 || s(i) > A2 )
        [r,c] = find(L==i);
        new(r,c) = 0;
    end;
end;
for i = 1:size(a)
    if(a(i)/b(i) < r1 || a(i)/b(i) > r2 )
        [r,c] = find(L==i);
        new(r,c) = 0;
    end;
end;
imtool(new,[]);
toc
End

```

Method2

Main function-

```
clear;
close all;
load('./data/radarsat2-tj.mat')
I_multilook = f_multilooking(I, 2, 2);
[I_prob, I_bw] = f_lognormal_mixture(I_multilook, 15, 10, 3,
0.0005);
figure, imshow(I_multilook,[]);
figure, imshow(I_prob);
figure, imshow(I_bw);
```

Multilook function-

```
function I_multilook = f_multilooking(I,az_look,rg_look)
    N_az = floor(size(I,1)/az_look);
    N_rg = floor(size(I,2)/rg_look);
    I_multilook = zeros(N_az,N_rg);
    for i = 1:N_az
        for j = 1:N_rg
            I_multilook(i,j) = mean2(I((i-1)*az_look+1:i*az_look,(j-
1)*rg_look+1:j*rg_look));
        end
    end
end
End
```

Log normal mixture function-

```
function [I_prob, I_bw] = f_lognormal_mixture(I, r_c, r_g, K,
Pf)
```

```

    I_log = log(I);
    I_log = padarray(I_log, [r_c, r_c], 'symmetric');
    [mrows,ncols] = size(I_log);
    ref_win = ones(2*r_c+1,2*r_c+1);
    ref_win(r_c-r_g+1:r_c+r_g+1,r_c-r_g+1:r_c+r_g+1)=0;
    index = (ref_win==1);
    I_prob = zeros(mrows, ncols);
    h = waitbar(0, 'Processing');
    for i=(r_c+1):(mrows-r_c)
        waitbar(i/mrows);
        for j=(r_c+1):(ncols-r_c)
            temp = I_log(i-r_c:i+r_c,j-r_c:j+r_c);
            x = temp(index);
            if j==(r_c+1)
                [mu,variance,weight,~] = fMyEM(x,K,20,0.01);
            else
                [mu,variance,weight,~] =
fMyEM(x,K,20,0.01,mu,variance,weight);
            end
            I_prob(i,j) =
sum(weight.*normcdf(I_log(i,j),mu,sqrt(variance)));
        end
    end
    close(h);

```



```

I_bw = I_prob > 1-Pf;
I_prob = I_prob((r_c+1):(mrows-r_c), (r_c+1):(ncols-r_c));
I_bw = I_bw((r_c+1):(mrows-r_c), (r_c+1):(ncols-r_c));
end

function [mu,variance,p,iterNum] =
fMyEM(X,numOfComponent,maxIter,tol,muInit,varianceInit,pI
nit)
X = X(:);
N = numel(X); % number of samples
K = numOfComponent; % number of components
if nargin==4
temp = randperm(N);
mu = X(temp(1:K));mu = mu(:);
clear temp;
variance = var(X) * ones(K,1);
p = (1/K) * ones(K,1);
end
if nargin==5
mu = muInit(:);
variance = var(X) * ones(K,1);
p = (1/K) * ones(K,1);
end
if nargin==6
mu = muInit(:);
variance = varianceInit(:);
p = (1/K) * ones(K,1);
end

```

```

if nargin==7
    mu = muInit(:);
    variance = varianceInit(:);
    p = pInit(:);
end
for i=1:maxIter
    G = repmat(p',N,1) ./ sqrt(repmat(variance',N,1)) .* exp(-
((repmat(X,1,K)-repmat(mu',N,1)).^2)
(2*repmat(variance',N,1)));
    g = sum(G,2);g=g(:);
    G = G./ repmat(g,1,K);
    M = sum(G,1); M = M(:); M = M + 1e-6; M = M/sum(M) *
N;
    muNEW = (G'* X) ./ M;
    varianceNEW = sum(G.*((repmat(X,1,K)-
repmat(muNEW',N,1)).^2),1)'/M + 1e-6;
    pNEW = M/N;
    if (norm(mu-muNEW,1)/norm(mu,1)<tol &&
norm(varianceNEW-variance,1)/norm(variance,1)<tol &&
norm(pNEW-p,1)/norm(p,1)<tol)
        break;
    end
    mu = muNEW;
    variance = varianceNEW;
    p = pNEW;
end
iterNum = i;
mu = muNEW;

```

```

    variance = varianceNEW;
    p = pNEW;
End

```

Method3

Main function-

```

clear;
close all;
load('./data/radarsat2-tj.mat')
I_multilook = f_multilooking(I, 2, 2);
[I_prob, I_bw] = f_semiparametric(I_multilook, 15, 10, 0.0005);
figure, imshow(I_multilook,[]);
figure, imshow(I_prob);
figure, imshow(I_bw);

```

Multilook function-

```

function I_multilook = f_multilooking(I,az_look,rg_look)
    N_az = floor(size(I,1)/az_look);
    N_rg = floor(size(I,2)/rg_look);
    I_multilook = zeros(N_az,N_rg);
    for i = 1:N_az
        for j = 1:N_rg
            I_multilook(i,j) = mean2(I((i-1)*az_look+1:i*az_look,(j-1)*rg_look+1:j*rg_look));
        end
    end

```

end

End

Semiparametric function-

```
function [I_prob, I_bw] = f_semiparametric(I, r_c, r_g, Pf)
    I_log = log(I);
    figure, imshow(I, []);
    title('Please drag a rectangle of sea clutter and double click to
    proceed')
    h = imrect;
    pos = wait(h);
    close;
    xmin = pos(1);
    ymin = pos(2);
    width = pos(3);
    height = pos(4);
    I_train = I_log(ymin:(ymin+height),xmin:(xmin+width)); %
    train samples
    N = numel(I_train);
    [bandwidth,~,~,~]=f_kde(I_train(:));
    [mrows_t,ncols_t] = size(I_train);
    I_unif = I_train;
    for i = 1:mrows_t
        for j = 1:ncols_t
            I_unif(i,j)
            =
            sum(normcdf(I_train(i,j),I_train(:),bandwidth))/N;
        end
    end
```

```

end
U1 = zeros(floor(mrows_t/3),floor(ncols_t/3));
U2 = zeros(floor(mrows_t/3),floor(ncols_t/3));
U3 = zeros(floor(mrows_t/3),floor(ncols_t/3));
U4 = zeros(floor(mrows_t/3),floor(ncols_t/3));
U5 = zeros(floor(mrows_t/3),floor(ncols_t/3));
U6 = zeros(floor(mrows_t/3),floor(ncols_t/3));
U7 = zeros(floor(mrows_t/3),floor(ncols_t/3));
U8 = zeros(floor(mrows_t/3),floor(ncols_t/3));
U9 = zeros(floor(mrows_t/3),floor(ncols_t/3));
for i = 2:3:mrows_t-1
    for j = 2:3:ncols_t-1
        tmp = I_unif(i-1:i+1,j-1:j+1);
        U1((i-2)/3+1,(j-2)/3+1) = tmp(2,2); % central pixel
        U2((i-2)/3+1,(j-2)/3+1) = tmp(1,1);
        U3((i-2)/3+1,(j-2)/3+1) = tmp(1,2);
        U4((i-2)/3+1,(j-2)/3+1) = tmp(1,3);
        U5((i-2)/3+1,(j-2)/3+1) = tmp(2,3);
        U6((i-2)/3+1,(j-2)/3+1) = tmp(3,3);
        U7((i-2)/3+1,(j-2)/3+1) = tmp(3,2);
        U8((i-2)/3+1,(j-2)/3+1) = tmp(3,1);
        U9((i-2)/3+1,(j-2)/3+1) = tmp(2,1);
    end
end
U1 = U1(:);
U2 = U2(:);

```

```

U3 = U3(:);
U4 = U4(:);
U5 = U5(:);
U6 = U6(:);
U7 = U7(:);
U8 = U8(:);
U9 = U9(:);
RHOHAT
copulafit('Gaussian',[U1,U2,U3,U4,U5,U6,U7,U8,U9]);
I_log = padarray(I_log, [r_c, r_c], 'symmetric');
[mrows,ncols] = size(I_log);
ref_win = ones(2*r_c+1,2*r_c+1);
ref_win(r_c-r_g+1:r_c+r_g+1,r_c-r_g+1:r_c+r_g+1)=0;
index = find(ref_win==1);
N0 = numel(index);
hCV = bandwidth*(N/N0)^(1/5);
Z = zeros(size(I_log));
T_MQD = zeros(size(I_log));
T_SPD = zeros(size(I_log));
h = waitbar(0, 'Processing');
for i=(r_c+1):(mrows-r_c)
    waitbar(i/mrows);
    for j=(r_c+1):(ncols-r_c)
        x = I_log(i-r_c:i+r_c,j-r_c:j+r_c);
        x = x(index);
        x = x(:);

```

```

    T_SPD(i,j) = sum(normcdf(I_log(i,j),x,hCV))/N0;
    Z(i,j) = norminv(abs(T_SPD(i,j)-eps),0,1);
end
end
close(h)
z = zeros(9,1);
for i=(r_c+1):(mrows-r_c)
    for j=(r_c+1):(ncols-r_c)
        z(1) = Z(i,j);
        z(2) = Z(i-1,j-1);
        z(3) = Z(i-1,j);
        z(4) = Z(i-1,j+1);
        z(5) = Z(i,j+1);
        z(6) = Z(i+1,j+1);
        z(7) = Z(i+1,j);
        z(8) = Z(i+1,j-1);
        z(9) = Z(i,j-1);
        if sum(z)<0
            T_MQD(i,j) = 0;
        else
            T_MQD(i,j) = z.*(RHOHAT\z);
        end
    end
end
end
I_prob = chi2cdf(T_MQD, 9);
I_bw = I_prob > 1-Pf;

```

```
I_prob = I_prob((r_c+1):(mrows-r_c), (r_c+1):(ncols-r_c));  
I_bw = I_bw((r_c+1):(mrows-r_c), (r_c+1):(ncols-r_c));  
end
```